# Fluid release from the subducted Cocos plate and partial melting of the crust deduced from magnetotelluric studies in southern Mexico: Implications for the generation of volcanism and subduction dynamics

H. Jödicke,[1,2] A. Jording,[1] L. Ferrari,[3] J. Arzate,[3] K. Mezger,[4] and L. Rüpke[5]

Received 21 March 2005; revised 29 January 2006; accepted 19 April 2006; published 17 August 2006.

[1] In order to study electrical conductivity phenomena that are associated with subduction related fluid release and melt production, magnetotelluric (MT) measurements were carried out in southern Mexico along two coast to coast profiles. The conductivity-depth distribution was obtained by simultaneous two-dimensional inversion of the transverse magnetic and transverse electric modes of the magnetotelluric transfer functions. The MT models demonstrate that the plate southern profile shows enhanced conductivity in the deep crust. The northern profile is dominated by an elongated conductive zone extending >250 km below the Trans-Mexican Volcanic Belt (TMVB). The isolated conductivity anomalies in the southern profile are interpreted as slab fluids stored in the overlying deep continental crust. These fluids were released by progressive metamorphic dehydration of the basaltic oceanic crust. The conductivity anomalies may be related to the main dehydration reactions at the zeolite → blueschist → eclogite facies transitions and the breakdown of chlorite. This relation allows the estimation of a geothermal gradient of ~8.5°C/km for the top of the subducting plate. The same dehydration reactions may be recognized along the northern profile at the same position relative to the depth of the plate, but more inland due to a shallower dip, and merge near the volcanic front due to steep downbending of the plate. When the oceanic crust reaches a depth of 80–90 km, ascending fluids produce basaltic melts in the intervening hot subcontinental mantle wedge that give rise to the volcanic belt. Water-rich basalts may intrude into the lower continental crust leading to partial melting. The elongated highly conductive zone below the TMVB may therefore be caused by partial melts and fluids of various origins, ongoing migmatization, ascending basaltic and granitic melts, growing plutons as well as residual metamorphic fluids. Zones of extremely high conductance (>8000 S) in the continental crust on either MT profile might indicate extinct magmatism.

**Citation:** Jödicke, H., A. Jording, L. Ferrari, J. Arzate, K. Mezger, and L. Rüpke (2006), Fluid release from the subducted Cocos plate and partial melting of the crust deduced from magnetotelluric studies in southern Mexico: Implications for the generation of volcanism and subduction dynamics, *J. Geophys. Res.*, *111*, B08102, doi:10.1029/2005JB003739.

## 1. Introduction

[2] Fluid release and melt production are characteristic subduction-related processes, and both can readily be recognized by enhanced electrical conductivity [e.g., *Jones*, 1993]. Electromagnetic methods like geomagnetic depth sounding (GDS) and magnetotellurics (MT) have therefore been used to gain insight into zones, where dehydration, migration of fluids or melting occur. Basic studies of this kind have mainly been conducted at the active continental margin along the west coast of North and South America including the subducting Juan de Fuca plate in Vancouver Island [e.g., *Kurtz et al.*, 1986, 1990] and in Oregon [e.g., *Wannamaker et al.*, 1989], the Nazca plate in South Bolivia and North Chile [*Schwarz and Krüger*, 1997; *Brasse et al.*, 2002], and the Pacific plate in New Zealand [*Ingham*, 1988]. All these studies combined reveal a variety of conductivity anomalies indicating that structural, p,T and petrological conditions may differ depending on the local subduction regime.

[1]Institut für Geophysik der Westfälischen Wilhelms-Universität Münster, Münster, Germany.
[2]Deceased 8 April 2005.
[3]Centro de Geociencias, Campo Juriquilla, Universidad Nacional Autónoma de México, Querétaro, México.
[4]Institut für Mineralogie der Westfälischen Wilhelms-Universität Münster, Münster, Germany.
[5]SFB 574 und IFM-GEOMAR, Leibniz-Institut für Meereswissenschaften an der Universität Kiel, Kiel, Germany.


0148-0227/06/2005JB003739$09.00

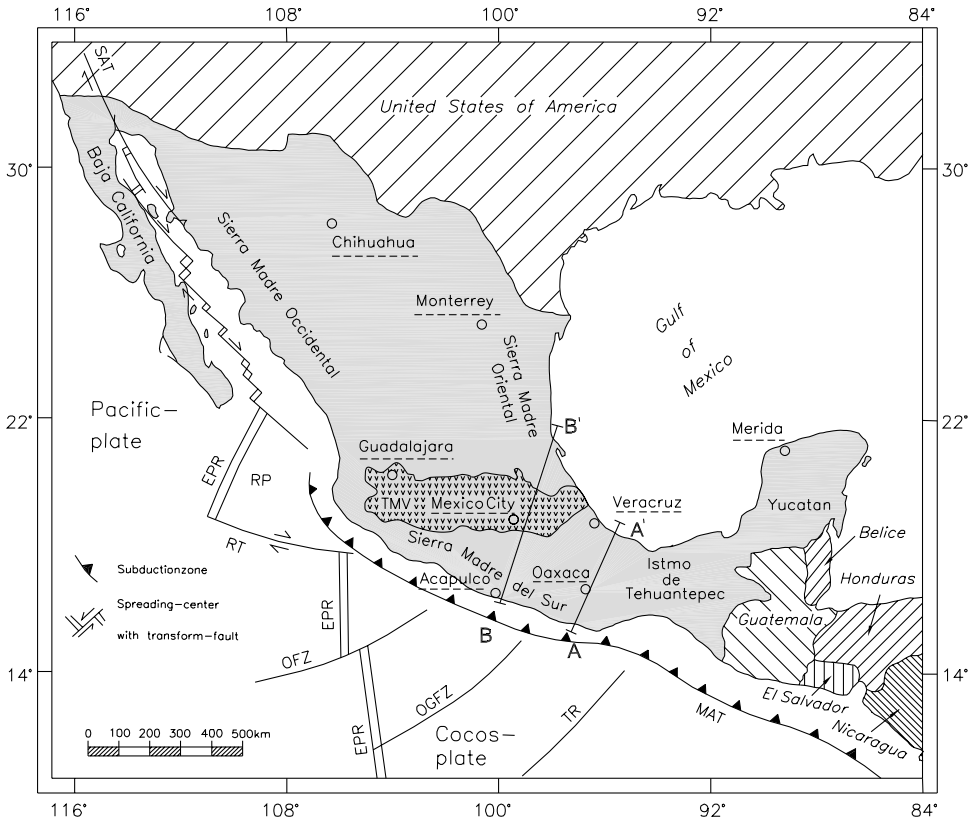


**Figure 1.** Simplified tectonic map of southern Mexico by *Campa and Coney* [1983], modified after *Böhnel* [1985], *Ortega-Gutierrez et al.* [1994], and *Pardo and Suarez* [1995]. Abbreviations are EPR, East Pacific Rise; MAT, Middle America Trench; OFZ, Orozco fault zone; OGFZ, O'Gorman fault zone; RP, Rivera plate; RT, Rivera transform fault; SAT, San Andreas transform fault; TMV, Trans-Mexican Volcano Belt; TR, Tehuantepec ridge. A-A′, B-B′ magnetotelluric profiles.

[3] A landward dipping zone of enhanced conductivity in the fore-arc region of the Juan de Fuca plate in Oregon was interpreted to directly image the free water content of subducted sediments and, thus to image the top of the plate itself [*Wannamaker et al.*, 1989]. Below Vancouver Island, a similar structure appearing above the slab may rather mirror the effect of ascending fluids released from the downgoing plate [*Kurtz et al.*, 1990]. This interpretation is in agreement with the results of experimental petrological studies during the last decade emphasizing the importance of dehydration reactions in the downgoing oceanic crust that accompany the transformation from metabasalt and gabbro to eclogite with increasing pressure and temperature [e.g., *Peacock*, 1993; *Tatsumi and Eggins*, 1995; *Schmidt and Poli*, 1998]. It is inferred that the released water is stored in the continental crust underneath an impermeable layer following the 450°C isotherm. In contrast, the storage of water associated with the formation of more or less horizontally layered structures seems to be impeded in the southern central Andes, probably due to the steep down bending of the Nazca plate favoring the formation of vertical faults instead, while the situation in New Zealand seems to lack any observable subduction related conductivity anomalies. The interpretation of the conductivity anomalies observed in the back arc regions is more difficult, because they may merge into regional or local, nonsubduction related conductivity structures of the continental crust. Age, and thus the thermal structure, of the subducting plate is the principal factor that influences the location of dehydration reactions [*Iwamori*, 1998; *Peacock and Wang*, 1999; *Kerrick and Connolly*, 2001; *Rüpke et al.*, 2004]. Indeed volcanism is abundant above "cold" subducting plates (age >15–20 Ma), but feeble or absent above young and "warm" plates in which dehydration occurs too early to meet the required p, T conditions for melting of the overlying mantle wedge [*Kirby et al.*, 1996; *Iwamori*, 1998]. Because of its age, which increases from ~14.5 Ma at longitude 102°W to ~19.5 Ma at longitude 97°W, the Mexican slab should be more akin to a warm subduction zone, however, andesitic-dacitic volcanism is common in the central Trans-Mexican Volcanic Belt (TMVB) (Figures 1 and 2).

[4] Generally, the Mexican subduction system of the Coos plate resembles the system of the Juan de Fuca plate. The most striking difference, however, is that the TMVB is oriented obliquely to the trench (Figures 1 and 2). This volcanism is thought to be related to the subduction of the Rivera and Cocos plates [*Nixon*, 1988; *Pardo and Suárez*, 1995; *Ferrari et al.*, 1999; *Wallace and Carmichael*, 1999; *Straub and Martin del Pozzo*, 2001; *García-Palomo et al.*, 2002a, 2002b]. However, the presence of alkaline oceanic island basalt (OIB)-type volcanism at Sierra Chichinautzin (Figure 2) as well as the absence of seismicity beneath the TMVB prompted several workers to develop genetic

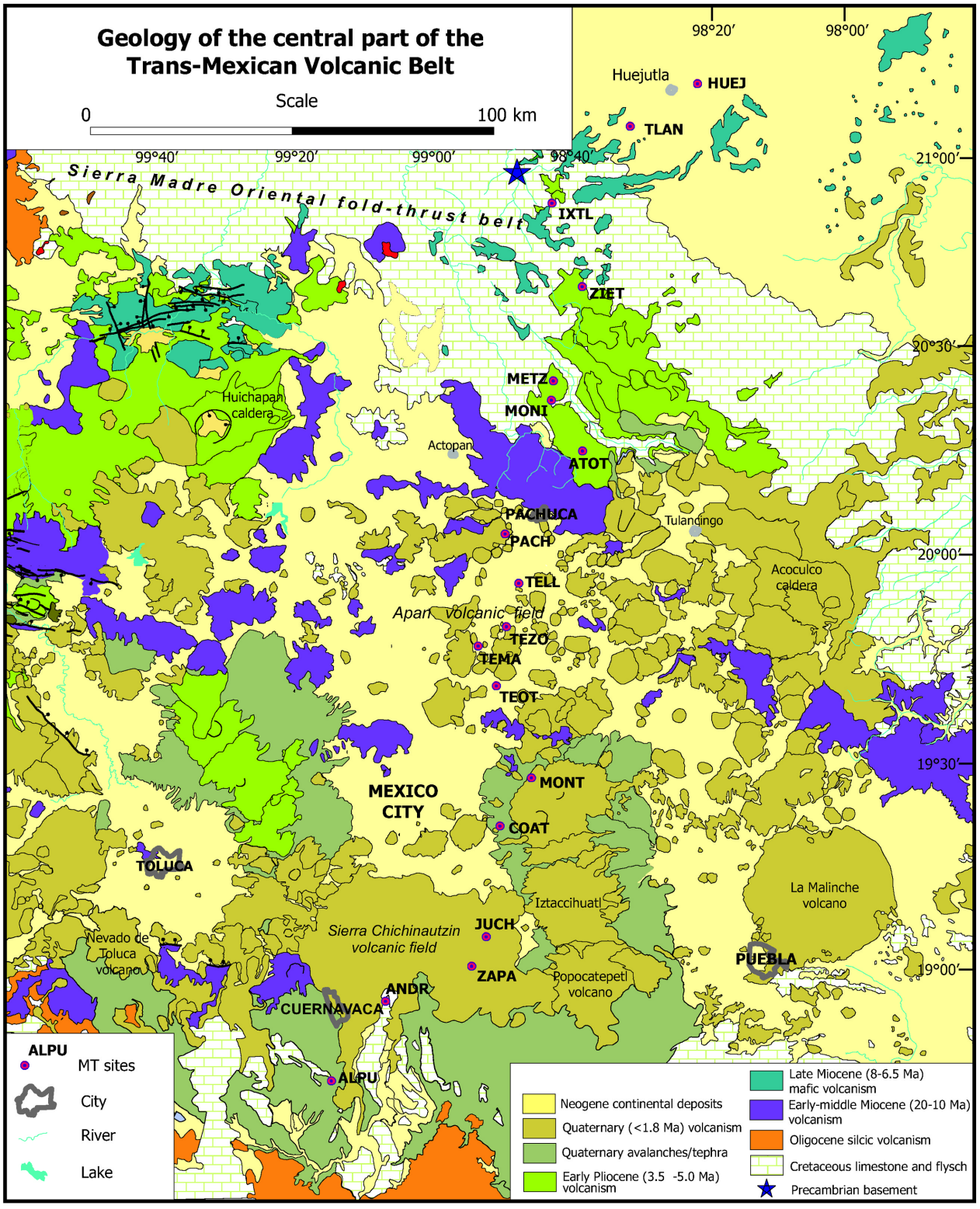


**Figure 2.** Geological map of the Trans-Mexican Volcanic Belt in the region crossed by the B-B′ MT profile; adapted from *Ferrari et al.* [2002].

models at variance with a classic subduction scenario [e.g., *Marquez et al.*, 1999; *Sheth et al.*, 2000].

[5] The oblique orientation of the TMVB offers the chance to study the conductivity distribution at depth along two profiles A-A′ and B-B′ for a better understanding why volcanism is generated on profile B-B′ but is almost absent on profile A-A′ (Figure 1). Profile A-A′ follows the Geotraverse of the Lithosphere in Mexico (GEOLIMEX) tran-

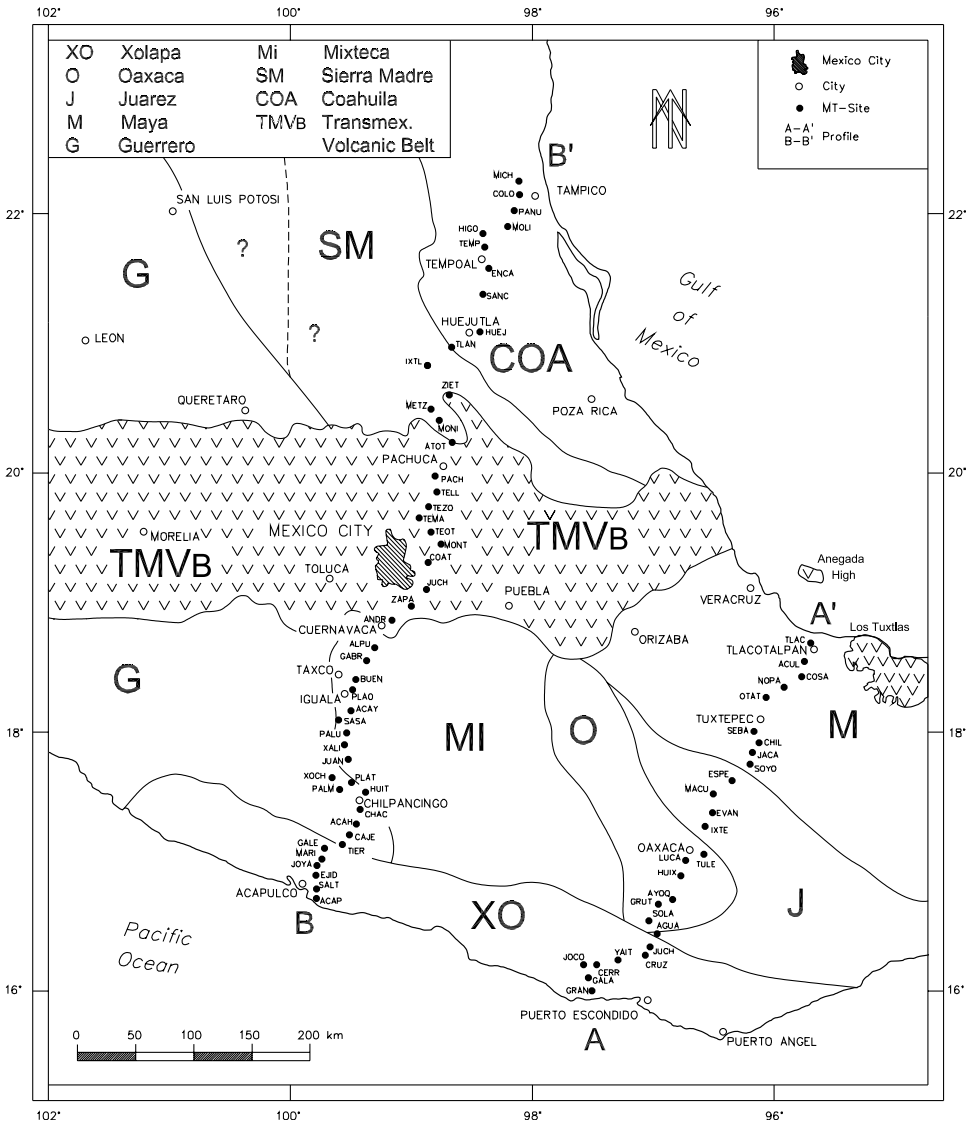


**Figure 3.** Locations of MT sites on profiles A-A′ (GEOLIMEX) and B-B′.

sect that was explicitly chosen for seismic reasons, because of the absence of recent volcanism [*GEOLIMEX Working Group*, 1994]. A geological model as well as results of refraction seismic and gravimetric studies are available for this line [*Spranger*, 1994, and references therein]. The second line B-B′ was added for comparative purposes in order to identify electrical signatures relevant to recent volcanism. The central part of profile B-B′ therefore crosses the TMVB near its active front represented by the Popocatépetl volcano. Gravimetric, but no refraction seismic data are available for this second profile [*Campos-Enríquez and Sanchez-Zamora*, 2000].

## 2. Magnetotelluric Study in Southern Mexico

### 2.1. Data Acquisition and Processing

[6] The magnetotelluric measurements carried out along two profiles A-A′ and B-B′ cross the whole subcontinent from the Pacific coast to the Gulf of Mexico (Figures 1 and 3). Profile A-A′ comprises 27 MT sites and runs from Puerto Escondido via Oaxaca to Tlacotalpan. Located 200 km to the northwest, profile B-B′ includes 48 MT sites from Acapulco to Tampico via Mexico City. Both profiles are oriented almost perpendicularly to the strike of the subducting Cocos plate and are thus perpendicular to the presumed main electrical features of the deep subsurface. These profiles were chosen in order to set up optimum conditions for two-dimensional (2-D) modeling.

[7] The MT data were obtained with different types of instruments. The Metronix EMF863μP system covers the period range from 0.25 to 4096 s (EMF863μP) and the Phoenix V5 system the period range from 0.0026 to 1820 s. On average, about 4 days of recording time were needed to reach sufficient data quality particularly at long periods. Site positions were obtained by means of GPS measurements. The estimation of sounding curves followed standard MT data processing methods including careful visual inspection of the selected time series (the latter was possible for the EMF863μP system only) in combination with coherency weighting procedures. Recordings at a base station for the

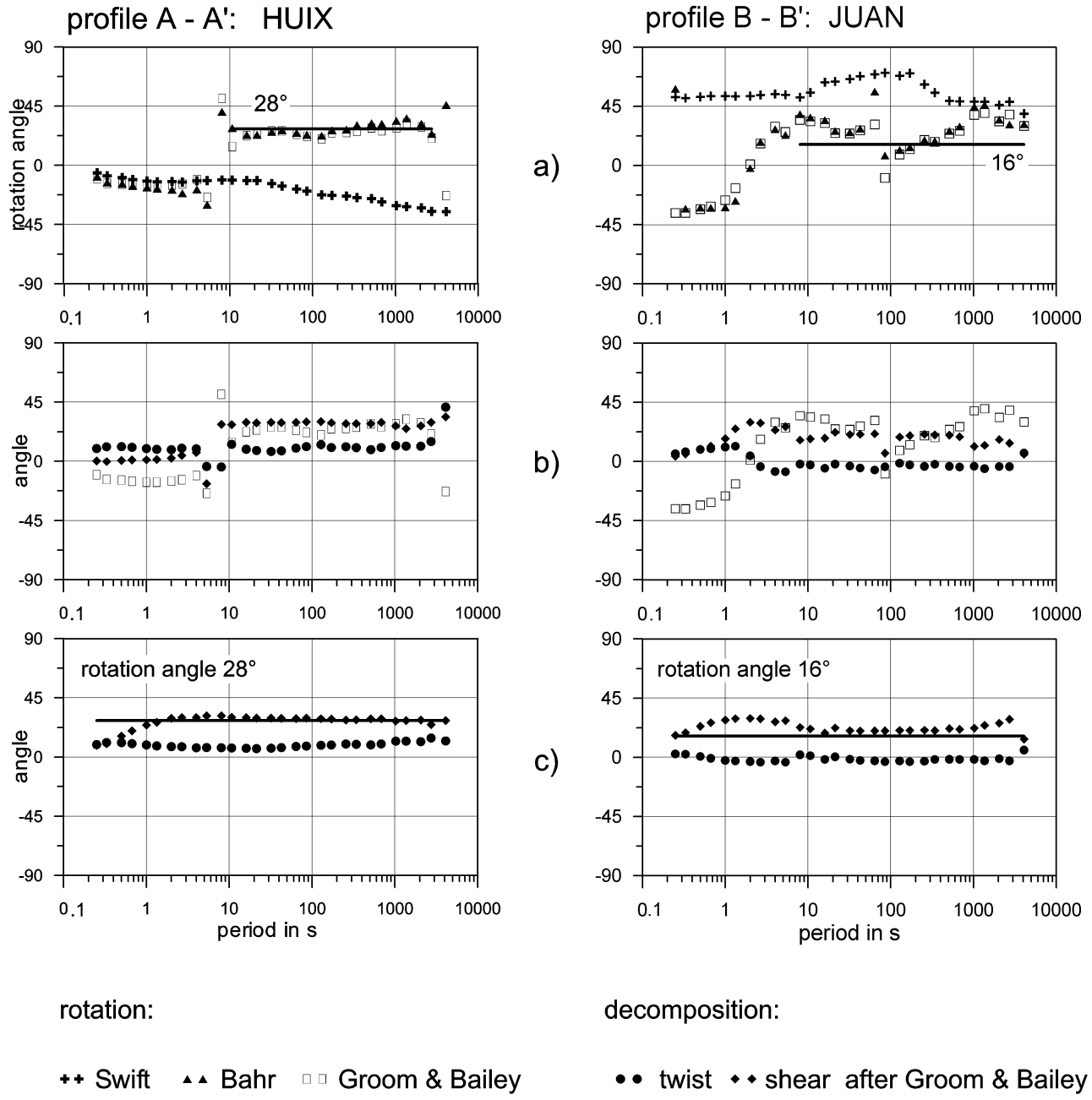


**Figure 4.** Decomposition of the MT impedance tensor of sites HUIX (profile A-A′) and JUAN (profile B-B′) using the methods of *Bahr* [1989, 1991] and *Groom and Bailey* [1989]. (a) rotation angles, the angles after *Swift* [1967] are shown for comparison; (b) Groom and Bailey's parameters "swift" and "shear" according to Figure 4a; (c) parameters swift and shear after optimum rotation.

remote reference technique were initially tried but given up after experiencing logistic problems.

[8] The crucial step in preparing 2-D modeling was the rotation of the tensors from the x, y (geographic) coordinate measuring system into a system of directions parallel and perpendicular to magnetotelluric strike, i.e., into the system of the transverse electric (TE) and transverse magnetic (TM) modes of polarization. We applied the decomposition methods of *Bahr* [1988, 1991] and *Groom and Bailey* [1989] that yield the correct strike from regional 2-D data distorted by local 3-D effects. Standard techniques of rotation to principal axes, e.g., by maximizing the expression $|Z_{xy}|^2 + |Z_{yx}|^2$, i.e., the sum of the squared off-diagonal elements of the magnetotelluric impedance tensor [*Swift*, 1967], were not adequate because "static shift" effects were found to exist at some sites. Such period-independent near-surface galvanic distortions shift the curves of apparent resistivity by an unknown real factor leaving the phases unchanged. As demonstrated by two examples, the decomposition resulted in rotation angles that are almost identical for Bahr's and Groom and Bailey's methods (Figure 4a). The observed period dependence of these angles is characteristic of the

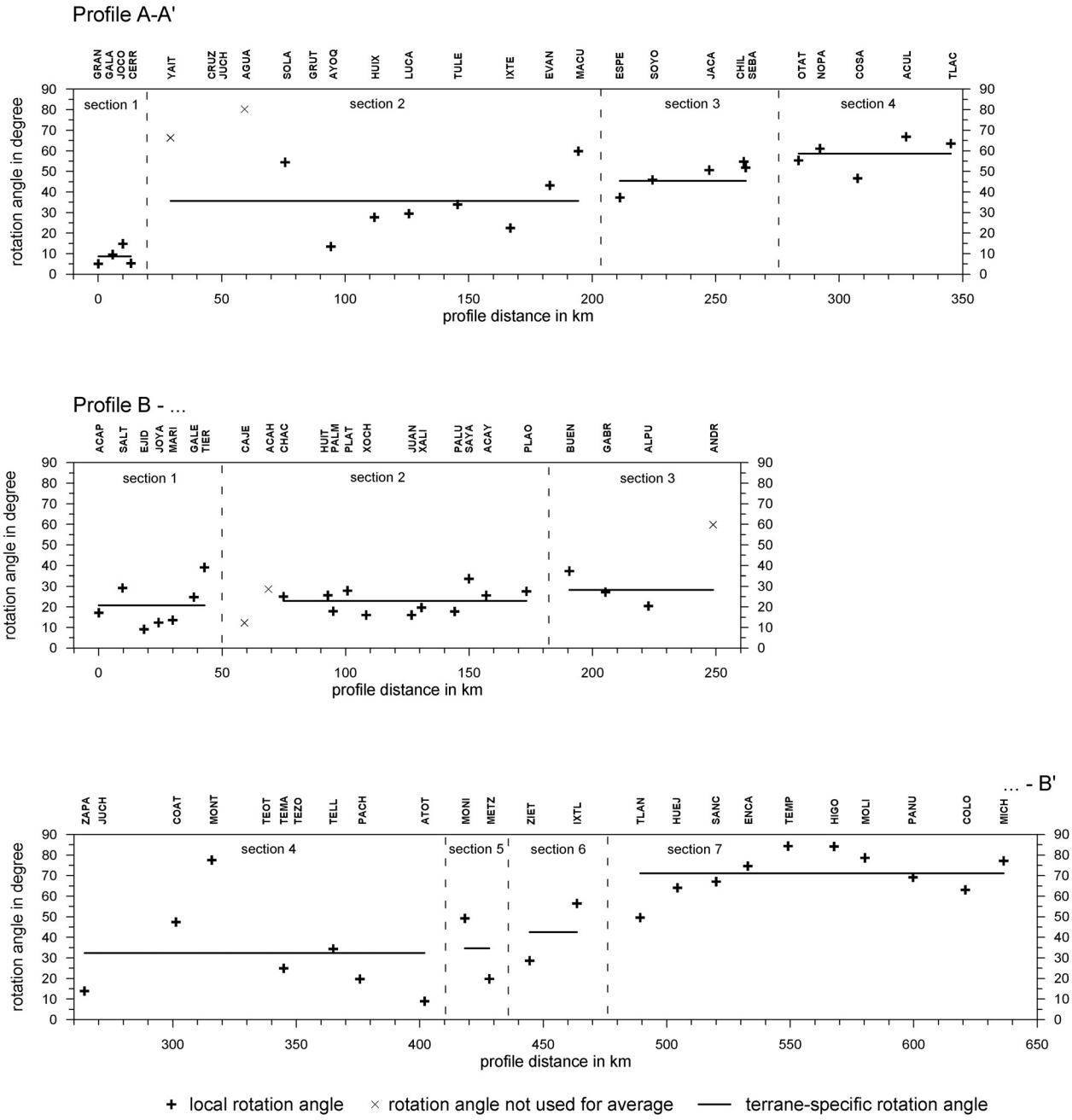


**Figure 5.** Optimum rotation angles, grouped to electrical units along profiles A-A′ and B-B′ [cf. *Jording et al.*, 2000].

majority of the sites but conflicts with strict 2-D behavior. In contrast, the Swift angles shown for comparison, are often much more stable, but biased by amplitude-shifted tensor elements. *Groom and Bailey* [1989] describe the local distorting effects by the parameters "twist" and "shear" of the impedance tensor. Figure 4b illustrates that unconstrained calculation of these parameters may exhibit frequency dependence as well. The finding of a rotation angle, which results in frequency-independent twist and shear, indicates that a regional 2-D strike is realized and the decomposition was successful. In most cases of this study the optimum rotation was reached by taking a constant rotation angle, averaged over the middle- and long-period range, or the long-period range only (Figure 4c). The use of averaged long-period rotation angles seems to be adequate, because long-period impedance properties are dominated by deep 2-D conductivity structures, which were intended to be preferably analyzed.

[9] The resulting rotation angles for MT profiles A-A′ and B-B′ (Figure 5) representing here the regional 2-D directions perpendicular to the magnetotelluric strike (TM mode), agree reasonably well with the NNE-ENE direction of the subduction of the oceanic Cocos plate underneath the North American plate [e.g., *Pardo and Suarez*, 1995].

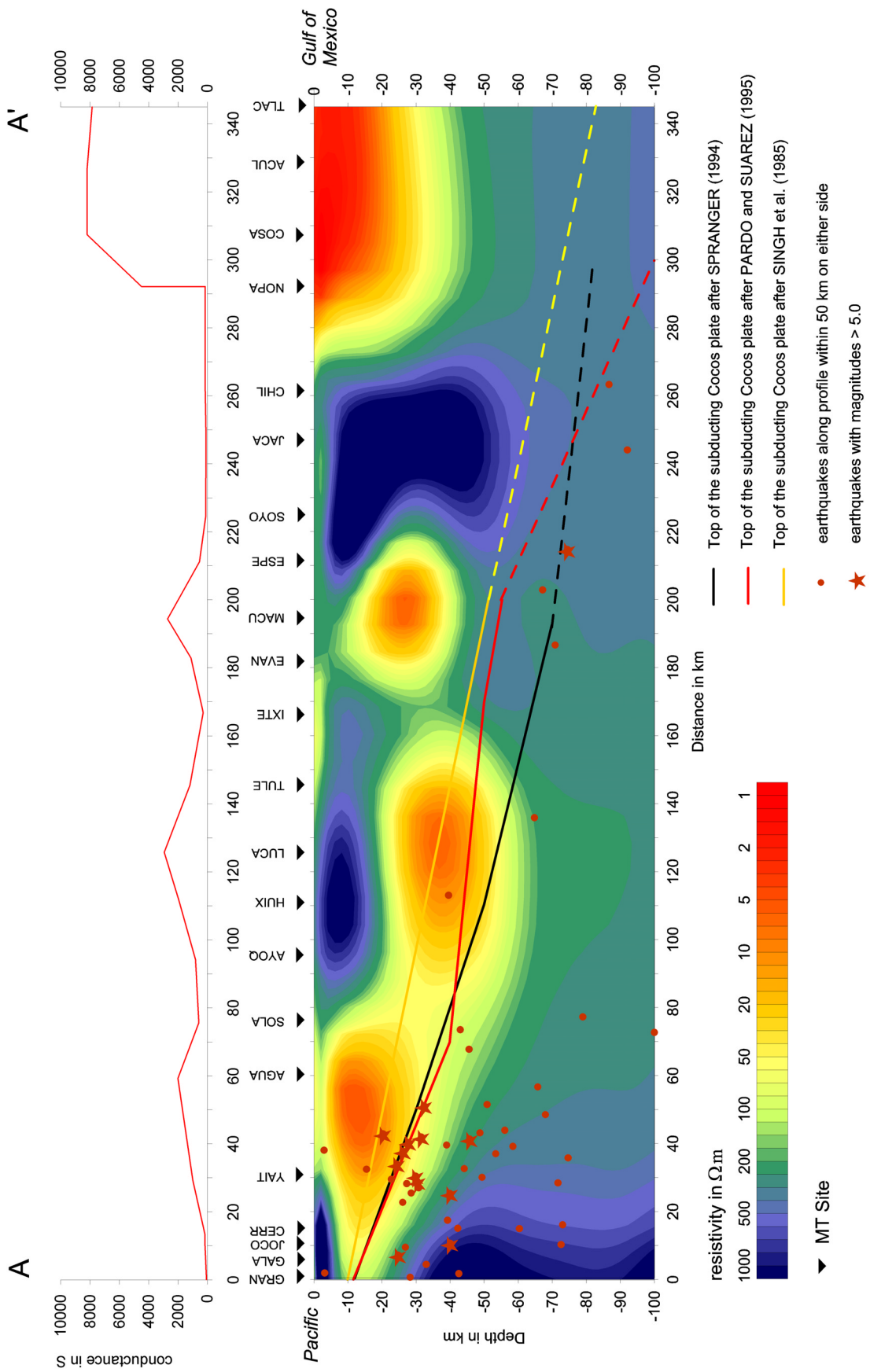


**Figure 6.** Profile A-A′: Results of inversion of E and B polarization data, using the 2-D code by *Rodi and Mackie* [2001], slightly smoothed compared to the original output. Earthquake hypocenters projected onto the profile from an area of 50 km on either side of the profile; data courtesy by M. Guzman. (top) Integrated conductivity (conductance in S).

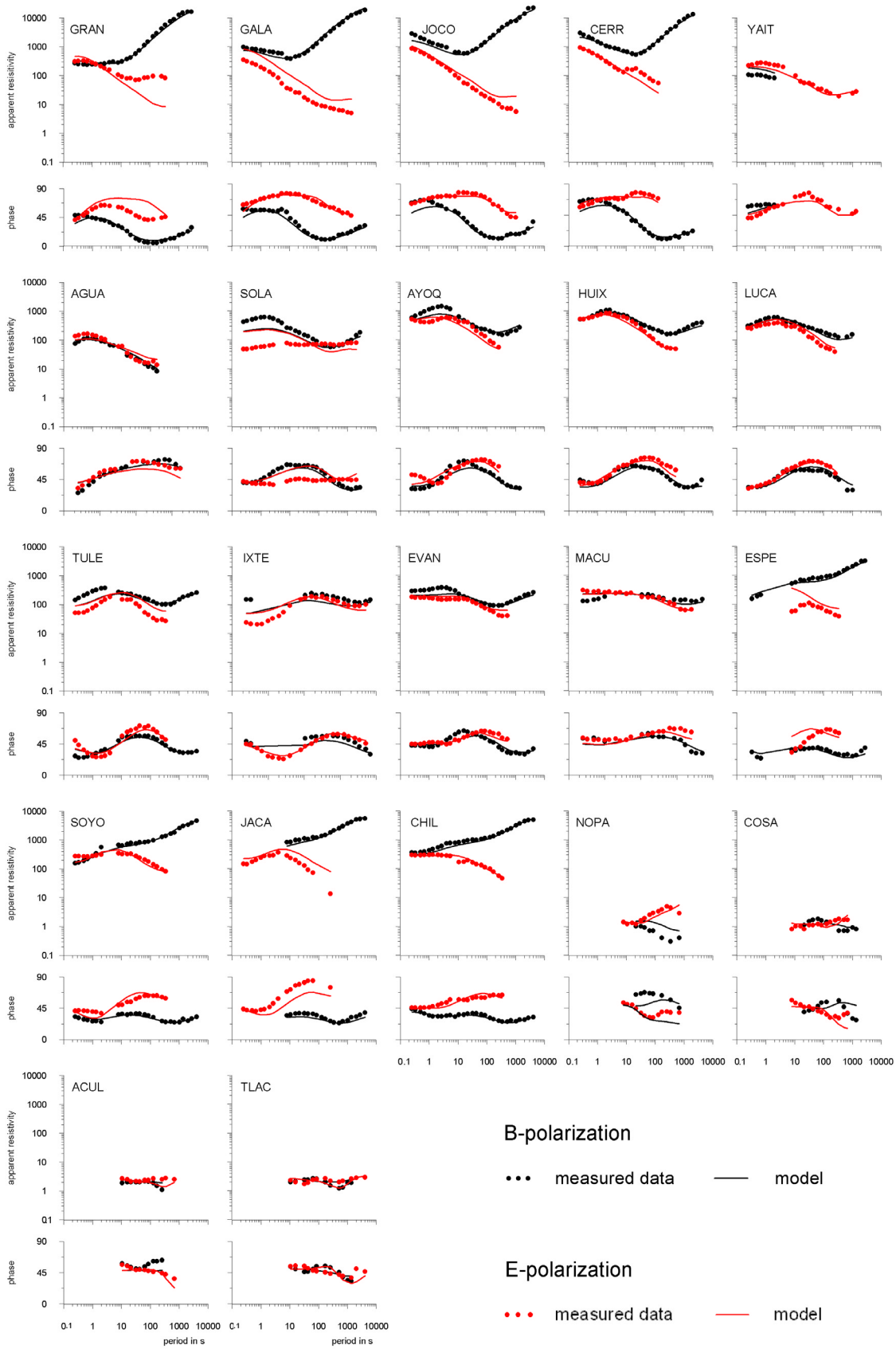


**Figure 7.** Profile A-A′; MT data used for modeling and model curves (black, TM mode; red, TE mode).

Dimensionality parameters like skewness, as defined by *Bahr* [1991], and anisotropy also indicate 2-D conditions to prevail, so that 2-D modeling of the data appeared generally justified. However, due to the extraordinary length of the two profiles (345 and 635 km) and the complex local and regional geotectonic environment, sections with different mean strike angles were defined along the lines (Figure 5). Detailed analyses demonstrated that these sections are characterized by groups of sounding curves, each with specific but similar shapes. Moreover, a striking correlation was observed between these electrically defined units and tectonostratigraphic terranes and their boundaries, which, in addition to subduction, are characteristic for the tectonic situation in southern Mexico [*Jording et al.*, 2000].

[10] Following decomposition, the static shift effects, if there was any, had to be removed from the sounding curves. For a test, whether static shift might be present, we simply compared the "amplitude sensitive" values of the rotation angles after *Swift* [1967] with the "phase sensitive" values after *Bahr* [1988, 1991]. If they were the same, it was assumed that no static shift was contained in the data. In addition, we compared the levels of similarly shaped apparent resistivity curves of neighboring sites within the various electrical units. In case of larger differences in level, static shift was considered as a possible reason. The static shift correction was then performed interactively during 2-D modeling. By comparison with 2-D model curves, the measured input apparent resistivity curves were shifted, if necessary, to improve the model fit and, particularly, to smoothen the deeper portions of the conductivity models, assuming that deep electrical structures tend to be laterally homogeneous.

### 2.2. Two-Dimensional Modeling

[11] For 2-D modeling, we used the 2-D inversion code by *Rodi and Mackie* [2001]. Except for tests, TM and TE modes were inverted simultaneously. The topography along the profiles was not considered.

[12] The result for profile A-A′ is shown in Figure 6. The model is based on a grid of 83 horizontal and 75 vertical blocks and a starting value of 500 Ω m half-space resistivity except for the left and right upper edges of the grid. Extending 150 km beyond the actual profile length on either side, the resistivity was set to 0.3 Ω m down to the corresponding water depths in order to allow for the influence of the sea and its possible "coast effects". The lower boundary of the model was fixed to 450 km. However, the choice of the starting model had little influence on the final result. The RMS error of the model fit was 6.87 according to the error definition by *Mackie et al.* [1997]. Measured and modeled data are shown in Figure 7. Here, only those measured data are displayed that were actually used as input for the model calculations.

[13] The main result of the calculations is that four clearly distinct zones of enhanced conductivity are encountered along profile A-A′ (Figure 6). Two of them, in the southwest, agree reasonably well with the result of an earlier MT study by *Arzate et al.* [1995]. The characteristic "cloudy" shapes of the conductivity anomalies are also generated by other 2-D inversion schemes [*Jording*, 2000]; they are by no means a special feature of the *Rodi and Mackie* [2001] algorithm. Particularly the RRI algorithm by *Smith and Booker* [1991], which in our experience emphasizes layered structures, if there were any, showed almost identical results.

[14] As it is not possible to estimate the individual thicknesses or conductivities of such conductors, because of MT equivalence relations, the corresponding conductance (integrated conductivity) values in [S] (conductivity [S/m] × thickness [m]) along the profile are added (Figure 6, uppermost section). Hence three of the conductive zones sum up to integrated conductivity values of about 2000 S. The fourth of them, close to the Gulf of Mexico, reaches from the surface down to more than 20 km and exhibits remarkably higher values of about 8000 S.

[15] The modeling of the profile B-B′ was performed in a similar way. Because of its length, it was split into two parts (Figure 8 (middle), sites ACAP–TEMA; Figure 8 (bottom), sites ZAPA–MICH), which overlap at 4 MT sites for better linking (Figure 8, top). Both grids contain 84 horizontal and 75 vertical blocks. In this case a 300 Ω m half-space starting resistivity was used, except for the respective edges, where the effect of the sea was accounted for. In comparison with profile A-A′, the values of the RMS errors turned out to be a little higher for profile B-B′ (7.81 for the southwestern, 7.73 for the northeastern part), which is in agreement with the somewhat lower quality of the measured data. On the southwestern part of profile B-B′ static shift was a major problem, because more than half of the TE and/or TM apparent resistivity curves had to be corrected, while this was necessary for a few curves only on its northeastern part and on profile A-A′.

[16] The model for profile B-B′ displays high conductive zones too but differs from A-A′ in several important aspects. Close to the Pacific coast, again a zone of increased conductivity is detected, but its conductance reaches 200 S only (Figure 8, top). Most significantly, in the central part of the profile an elongated anomalous high-conductivity structure is found at continental middle and lower crustal depths extending over more than 300 km underneath and beyond the TMVB. This central anomaly exhibits an average integrated conductivity of about 3000 S reaching locally more than 4000 S. In the northeastern part of the profile up to the Gulf of Mexico a conductive surface layer occurs in a position corresponding with the remarkable conductor at the end of profile A-A′ but showing much smaller conductance values of about 560 S only.

## 3. Discussion

### 3.1. Location and Nature of the Zones of Enhanced Conductivity

[17] In order to define the spatial relation between the zones of enhanced conductivity and the subducting plate, the conductivity sections are displayed together with the top of the plate derived from the refraction seismic experiment along the GEOLIMEX profile [*Spranger*, 1994] and/or seismological data [*Singh et al.*, 1985; *Suarez et al.*, 1992; *Pardo and Suarez*, 1995; *Valdez-Gonzalez and Meyer*, 1996] (Figures 6 and 8). A collection of focal depths of earthquakes that have occurred underneath a band of 50 km on either side of the MT profiles is shown as well. These earthquakes define a zone of flat subduction near the coast, but toward greater depths the downgoing plate is seismo-

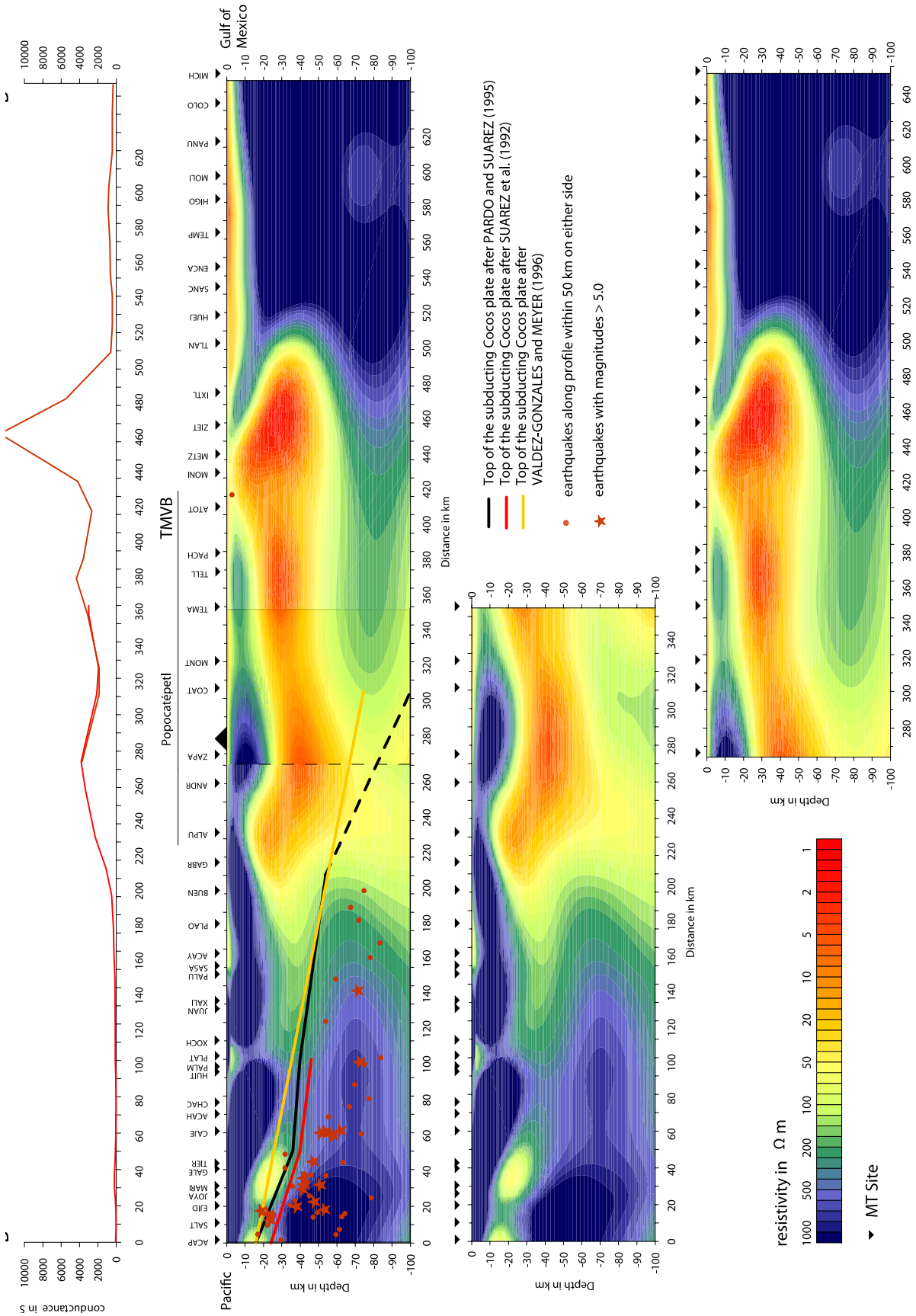


**Figure 8.** Profile B-B′; result of inversion, earthquake distribution, and integrated conductivity as for profile A-A′ (Figure 6). Earthquake hypocenters projected onto the profile from an area of 50 km on either side of the profile; data courtesy by M. Guzman. (top) Integrated conductivity (conductance in S).

logically not well constrained, because only few earthquakes have been recorded along profile A-A′ and no earthquake has been recorded in the mantle underneath the TMVB along profile B-B′ [*Pardo and Suarez*, 1995]. Except for the models of *Singh et al.* [1985] and *Valdez-Gonzalez and Meyer* [1996], all conductive zones seem to be located clearly above the subducting plate in the deeper parts of the continental crust. Moreover, assuming that the refraction seismic experiment [*Spranger*, 1994] may yield the most reliable depth information about the slab for profile A-A′, and the seismological data by *Pardo and Suarez* [1995] for profile B-B′, it becomes obvious that most of the conductivity anomalies may ground on, or, originate from the top of the plate (Figures 6 and 8). The southwestern part of the elongated anomaly below the TMVB even gives the impression of tracing the seismologically inferred down bending of the plate.

[18] In the following discussion about the nature of the conductivity pattern along the MT profiles we focus on subduction-related fluids and partial melts but start with the question of whether other subduction related sources might offer reasonable alternative explanations. It is striking, for example, that the rich copper provinces of the Earth follow the Tertiary and Cretaceous subduction zones [*Russell*, 1992]. In particular Fe-, Cu-, or Zn-sulfide or oxide rich ore deposits, that formed by precipitation from hydrothermal fluids associated with granodioritic batholiths or stocks [*Russell*, 1992], might be candidates for producing areas of high conductivity. Large volumes of such ores are known to form finely disseminated impregnations in the epithermal zone of intrusions, but deposits forming vein systems or fractures fillings are also known. These deposits would be of major interest, because they can increase the bulk conductivity very effectively (cf. A. Jording et al., Ein- und zweidimensionale Auswertung audiomagnetotellurischer Daten über einem Dazit-Porphyrstock in Pulacayo (Bolivien), internal report, 1998). Large-scale formations of highly conductive clay minerals and propylitic alterations in the outer parts of the hydrothermal alteration zones of such intrusions may be another source of increased conductivity. Because of their large volumes they may be even more important than the vein-type ores. Since all these formations are limited to the p,T conditions of the uppermost few kilometers of the continental crust, highly conductive bodies of these kinds cannot account for the conductivity anomalies detected in the deep crust along the MT profiles.

[19] Even for the subducting crust itself, high conductivity caused by other sources than fluids has to be considered. Metal sulfides, in particular lenses of massive pyrite may be deposited along ocean ridges (''black smokers''). These ''Cyprus-type'' ores may not necessarily be scraped off the subducting plate [*Russell*, 1992], but may be transported to greater depths where they could mark the position of the downgoing plate. In rare cases high conductivity might even be attributed to carbon. Meta-anthracitic relics of kerogen and graphite as the final residues of the metamorphic combustion of organic matter ($C_{org}$) are well known to cause enormous conductivity anomalies in the upper continental crust. Under normal circumstances conductors of this type would not be expected in the subduction realm, because well oxidized deep ocean sediments preserve only about 1% $C_{org}$ which is much too little to have a measurable effect on electrical conductivity. However, the Ocean Drilling Project (ODP) encountered layers with more than 60% $C_{org}$ indicating anaerobic turnovers of the deep ocean circulation system (''black shale events'') [e.g., *de Graciansky et al.*, 1984]. During subduction, the carbonaceous matter contained in such layers would gradually be transformed into graphite in a process which is closely related to the origination of good conductors from typical upper crustal marine black shale horizons. Similar to the formation of graphitic shear zones in the upper and middle continental crust [cf. *Jödicke et al.*, 2004], subduction-related shearing may support local concentrations of this graphite, forming hereby highly conductive complexes. The existence of subducted graphite has been documented by graphitic samples that have been recycled back to surface by rising magmas.

[20] Because of the discontinuous conductivity pattern along the measured MT profiles (Figures 6 and 8), the existence of any measurable amounts of metal sulfides or graphite mineralizations that could mark the top of the oceanic crust appears unlikely. The distinct anomalies as a whole appear to be too shallow to be correlated with the subducting plate, particularly at some distance from the coast, provided its seismically or seismologically defined depth is correct. We may therefore exclude the possibility that the plate itself is seen electrically in our MT results. As a consequence, the plate itself does not show up by its water content, either. Obviously, the downgoing oceanic crust does not contain the necessary quantities of interconnected free water (brines) to be observable. For the given depth range this is in good agreement with results from *Peacock* [1990], who showed that free water in the near-coastal part of the subducting crust will almost completely be squeezed out from open pores and cracks of sediments and basalt in the depth range of <10 km up to 40 km due to lithostatic pressure increase. For this reason we will restrict the discussion to the concept of high-conductivity zones in the near-trench part of the subduction being caused by ascending fluids released from the downgoing plate [cf., e.g., *Kurtz et al.*, 1986, 1990; *Wannamaker et al.*, 1989; *Schwarz and Krüger*, 1997]. This concept is consistent with numerical models of dehydration at young subduction zones [e.g., *Iwamori*, 1998; *Rüpke et al.*, 2002].

### 3.2. Fluid Release

[21] Subduction-related metamorphism is central to the understanding of possible processes involved in the release of fluids during prograde metamorphism. Mineralized water (brines), stemming either from water-filled open pores and fractures, or from crystal (chemically bound) water of the oceanic crust, stand here for fluids, because COH fluids other than water do not contribute much to conductivity. Generally, the main metamorphic reactions associated with subduction modify an oceanic crust that was strongly affected by earlier seafloor metamorphism and strong hydrothermal alteration of the young basalts at the mid-ocean ridges due to deep-reaching seawater circulation. The alteration results in high porosity as well as in a zonation of hydrated minerals ranging from top to bottom of the oceanic crust from zeolite facies to prehnite-pumpellyite facies to greenschist facies. Close to crustal magma chambers even amphibolite and granulite facies conditions may be reached

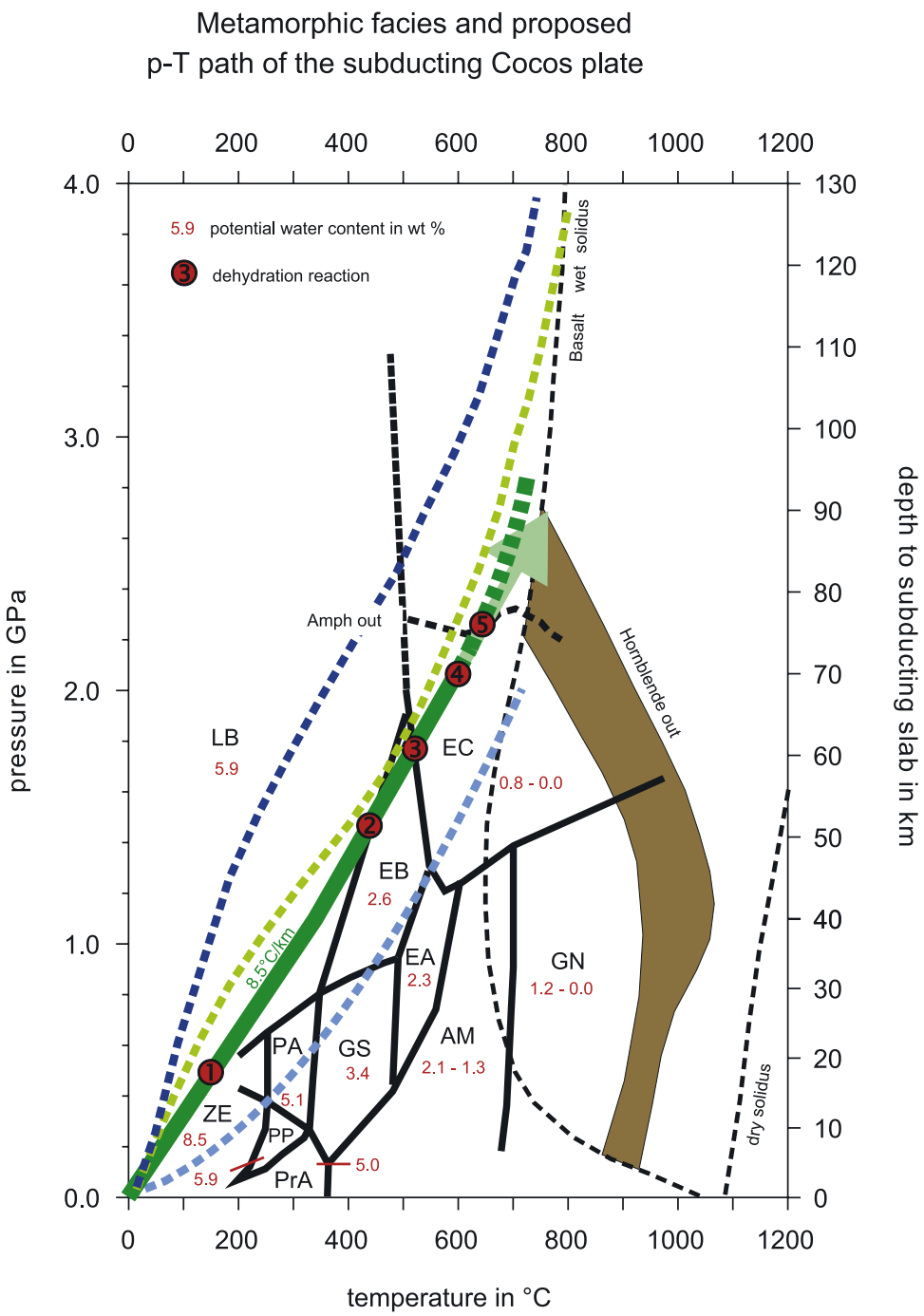


**Figure 9.** P,T conditions at the top of the subducting Cocos plate as proposed from the assumed relation between facies transitions and observed conductivity anomalies (dark green line). In comparison, geotherms are shown as adopted for the Cocos plate from thermal models by *Peacock* [1996] (modified from p-T path 2 in his Figure 4B, dashed light blue line) and from the thermal model shown in Figure 10 after *Rüpke et al.* [2002] (dashed bright green line). The dashed dark blue line results from the same model but excludes the effect of moderate shear heating (see text). The pressure-temperature diagram of metamorphic facies for a fully hydrated basaltic bulk composition is compiled from *Peacock* [1993], *Peacock et al.* [1994], and *Schmidt and Poli* [1998]. Metamorphic facies abbreviations are AM, amphibolite; EA, epidote-amphibolite; EB, epidote-blueschist; EC, eclogite; GN, granulite; GS, greenschist; LB, lawsonite-blueschist; PP, prehnite-pumpellyite; PrA, prehnite-actinolite; PA, pumpellyite-actinolite; ZE, zeolite facies. Note that the segmented depth scale is linearly converted from pressure due to crustal density 2.8 g $cm^{-3}$ for 0–40 km depth after *Ramirez-Ruiz* [1994] and to mantle density 3.3 g $cm^{-3}$ for depths >40 km, assuming a constant thermal gradient 8.5°C $km^{-1}$ of the Cocos plate.

[*Spear*, 1993]. From observations it is generally accepted that the oceanic crust is fully hydrated, at least in its upper basaltic part, while its deep, gabbroic part may be only partially (20–30%) hydrated [*Schmidt and Poli*, 1998]. In case of strong fracturing along the ridge and intense ''bend faulting'' during trench–near-plate bending, also the uppermost oceanic mantle may become partially hydrated by serpentinization [*Ranero et al.*, 2003].

[22] The dependence of water budget and dehydration reactions on age (cooling), dipping angle, convergence rate, thermal conductivity, shear heating, and bulk composition of the subducting oceanic crust and the thermal structure of the continental and oceanic plate, have been intensely studied by petrologists [e.g., *Peacock*, 1990, 1993; *Poli and Schmidt*, 1995, 2002; *Schmidt and Poli*, 1998]. According to experiments as well as numerical modeling, the release of structurally bound water from hydrated minerals of the subducting crust follows the sequence of metamorphic mineral facies as shown in Figure 9. The potential water content in wt % for each of the given facies in a fully hydrated basaltic oceanic crust is indicated by red numbers. From Figure 9, both the depths and the amounts of water released by dehydration reactions can be estimated if the p-T path of the downgoing crust is known.

### 3.3. Thermal Structure

[23] In order to link the observed conductivity anomalies with specific dehydration reactions, the thermal structure of the Mexican subduction zone was constrained using a thermomechanical model that solves for temperature and mantle flow [*Rüpke et al.*, 2004], following hereby a similar modeling approach as recently presented by *Manea et al.* [2005]. To initialize the thermal solution of the incoming plate, the standard half-space model for 15 Ma old oceanic lithosphere was used; for the continental plate the thermal gradient was set to 20°C/km in the top 40 km and of 10°C/km below with radiogenic heating active in the continental crust. For the flow solution the subduction velocity (7 cm/yr) along the slab surface was prescribed, and a simple temperature-dependent Newtonian viscosity model assumed.

[24] The model geometry was closely adapted to transect A-A′ which is fairly well known from seismic data to approximately 70 km depth (solid black line in Figure 6) whereas at greater depths the uncertainty on the slab's position increases (dashed black line in Figure 6). The thermal solution is summarized in Figure 9 where the calculated slab surface temperatures are plotted (dashed dark blue line). The slab surface temperatures show the typical S shape when plotted versus depth but can roughly be approximated by a linear geothermal gradient of about 6°C/km. Our calculated geotherm thus represents a fairly normal pressure dominated cold geotherm that is consistent with earlier models [e.g., *Peacock and Wang*, 1999]. Regarding the system of metamorphic mineral facies shown in Figure 9, this geotherm traverses mainly the lawsonite-blueschist (LB) field at shallow depths and intersects the blueschist → eclogite facies transition almost at the depth of the amphibolite-out reaction at about 2.4 GPa. Therefore the only significant dehydration event would be expected at depths ≥75 km. In contrast, the observed conductivity pattern along profile A-A′ rather suggests the presence of distinct dehydration reactions at shallower depths, especially in the depth range of 45 to 60 km (Figure 6); their interpretation would require remarkably higher thermal gradients. To overcome the crucial problem of underestimated temperatures in our geothermal model, the locations of conductivity anomalies along profile A-A′ (Figure 6) were, in a heuristic approach, directly correlated with major dehydration reactions in the underlying oceanic crust (Figure 9), taking its depth from seismic refraction results. Thus the sequence of distinct zones of increased conductivity along the profile are best accounted for if they are related stepwise to water release at the lawsonite blueschist (LB) → epidote blueschist (EB) → eclogite (EC) facies transitions and to the breakdown of chlorite at ≥600°C. This ''manual best fit'' yields a moderate thermal gradient of about 8.5°C/km for the top of the subducting oceanic crust at depths <70 km (dark green line, Figure 9).

[25] The result of the manual best fit opens the chance to estimate the amount of additional heat, which is needed to obtain a moderate geothermal gradient of 8.5°C/km. The source of this heat can be shear heating, latent heat of serpentinization reactions or, as suggested by *van Keken et al.* [2002], strong upwelling of hot mantle material toward the trench as a result of wedge convection. Shear heating is widely used in modeling the thermal structure of subduction zones, but had been explicitly disregarded during our first modeling tests, due to petrological considerations. For example, exhumed eclogites show little evidence of pervasive shearing which would be expected as an effect of shear heating. Instead, in subduction zones apparently most of the shear movement is taken up by localized shear zones as seen particularly well in the high-pressure rocks of the Bergen arcs [*Boundy et al.*, 1992; *Austrheim and Boundy*, 1994]. However, to demonstrate the effect of shear heating and to constrain the amount of additional heat that is necessary to shift the calculated cold geotherm to the moderate value of 8.5°C/km, the new model accounts for shear heating. Within the brittle domain, shear heating can be calculated from the equation $Q_{sh} = \tau\nu$ in units of W/m$^2$, where $\tau$ is the shear stress and $\nu$ is the fault's sliding velocity [e.g., *Wang et al.*, 1995]. The magnitude of the pressure-dependent shear stress can be determined at the base of Byerlee's friction law: $0.85*\sigma_n*(1-\lambda)$, where $\sigma_n$ is the lithostatic pressure and $\lambda$ the pore pressure ratio here assumed to be 0.98. We further assume that shear heating is only important to a depth of 70 km, where the subducting slab starts to be exposed to the hot mantle wedge. We thus obtain a maximum shear stress of ~38 MPa. Shear heating is implemented numerically as a ''pseudoductile'' volumetric heating rate by using the standard viscous heating equation $Q_{sh} = \tau * \varepsilon$ and assuming a shear zone width of 800 m. This results in a maximum viscous heating rate of ~107 $\mu$W/m$^3$.

[26] Figure 10 shows the thermal solution of the model that includes shear heating; the corresponding slab surface temperatures are plotted in Figure 9 (dashed bright green line). They show that this moderate amount of shear heating allows finding a geothermal gradient that coincides fairly well with the ''manual best fit''. The close match between the modeled geotherm and the fitted geotherm supports the assumption that a geothermal gradient of 8.5°C/km is reasonable.

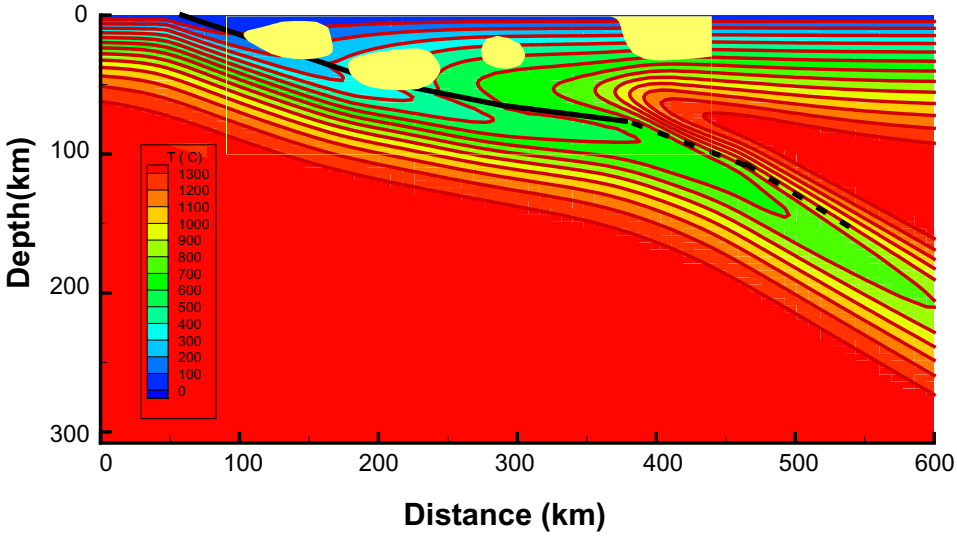


**Figure 10.** Thermal structure of subducting Cocos plate along profile A-A′ after *Rüpke et al.* [2004]. Conductive zones are added from Figure 6.

### 3.4. Conductivity Structure and Dehydration Reactions Along Profile A-A′

[27] The conductivity distribution along profile A-A′ can be interpret in more detail using the estimated thermal gradient of about 8.5°/km. In our model the first zone of enhanced conductivity 1 (Figure 11, km 10–70) is assumed to originate from free water that is expelled from gradually closing fractures and open pore spaces in the oceanic crust. Further contributions to the water budget at these shallow depths come from early dehydration reactions starting with the breakdown of clay minerals and their gradual transformation to smectites and possibly micas at temperatures of 50° to 150°C [*Peacock*, 1990; *Rüpke et al.*, 2002]. These reactions are followed by the stepwise decomposition of the zeolite minerals to feldspars and water in the basaltic crust. These reactions proceed until the blueschist facies is reached (dehydration reaction 1 in Figure 9 represents one example for these mostly continuous reactions). The blueschist facies, including lawsonite-blueschist (LB) and, at higher temperatures, epidote-blueschist (EB) facies, are characterized by the hydrous mineral assemblage lawsonite-glaucophane-chlorite-albite/jadeitic clinopyroxen ± phengite, among which lawsonite (7 to 15 wt % of MOR basalt) and chlorite (5–30 wt %) have the highest $H_2O$ contents with up to 11.2 wt % and 12 wt %, respectively [*Schmidt and Poli*, 1998]. The water from lawsonite is released beyond the intersections of the lawsonite blueschist/epidote blueschist boundary (dehydration reaction 2, depth ~50 km, 3.3 wt % water potential) and is correlated with the conductive zone 2 in Figure 11. The high water potential of this reaction may be the cause for the broad shape of the corresponding conductivity anomaly which may extend to profile distance >140 km. The pore water potential of sediments is quantitatively unimportant here [*Schmidt and Poli*, 1998]. The epidote blueschist/eclogite boundary (dehydration reaction 3, depth ~60 km, 1.8 wt % water potential), defined by the dehydration of glaucophan + clinozoisite [*Evans*, 1990], is related to the conductive zone 3, whereas the following conductive zone 4 is associated with the discontinuous breakdown of chlorite at ~600°C (reaction 4) [*Poli and Schmidt*, 2002]. The Moho depth based on gravimetric data by *Ramirez-Ruiz* [1994] indicates that this conductive zone is located in the lower continental crust which is consistent with its isolated appearance. Because of the lack of any impermeable layer, ascending water cannot be stored in the mantle, nor underneath the Moho, but reacts with the dry lower crust.

[28] The expected next dehydration step in our model is the decomposition of amphibole at pressures >2.2 GPa (reaction 5, 20–60 wt % of basalt, ~0.6 wt % $H_2O$). This reaction cannot be linked to any conductivity anomaly in our model. On the contrary, the continental crust is highly resistive between km 220 and km 270 on profile A-A′ where the slab may have reached depths >75 km (resistive zone V), sufficient to decompose amphibole. In contrast to chlorite, the rather small amounts of water liberated from the breakdown of amphibole may be consumed by hydration of peridotite in the 50 km thick and relatively cold part of the mantle wedge overlying the subducting crust [cf. *Iwamori*, 1998, Figure 6; *Schmidt and Poli*, 1998].

[29] The last conductive zone VI at the northeastern end of profile A-A′ comprises the depth range of the whole continental crust. Characterized by its maximum integrated conductivity, it is obviously unrelated to any of the trench–near-dehydration processes described so far. At least the upper 3–4 km (conductive zone VIa) of the total conductance may originate from Tertiary marine terrigeneous sediments of the Tampico-Misantla basin, which represents the landward extension of the Gulf of Mexico basin. However, these rocks may become more resistive at greater depth. It appears unlikely, that any electrolytically conducting sediments are capable of producing the observed high conductance values at depth over 4 km (conductive zone VIb).

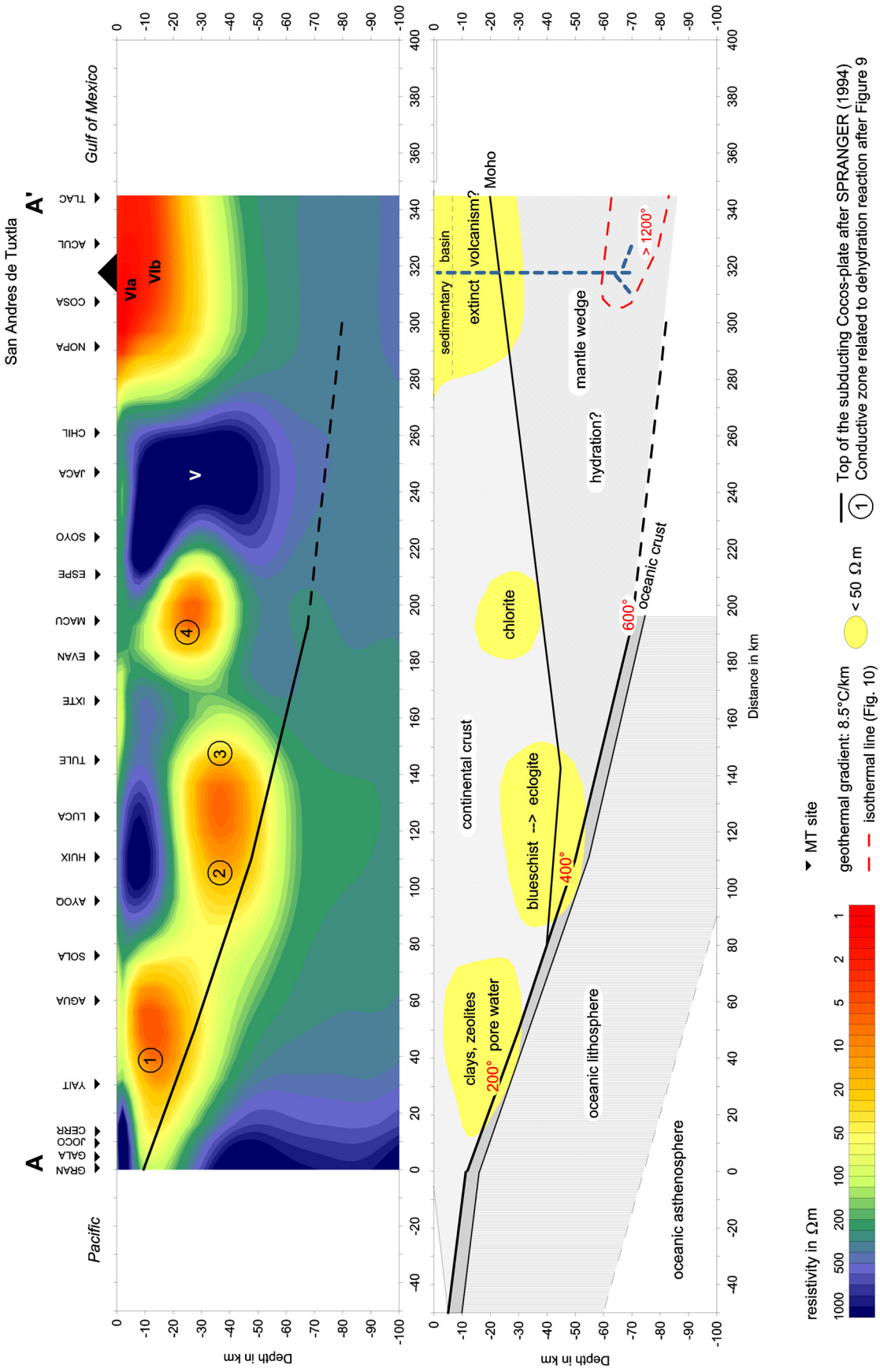


**Figure 11.** Schematic petrological interpretation of conductivity anomalies along MT profile A-A′ (see text).

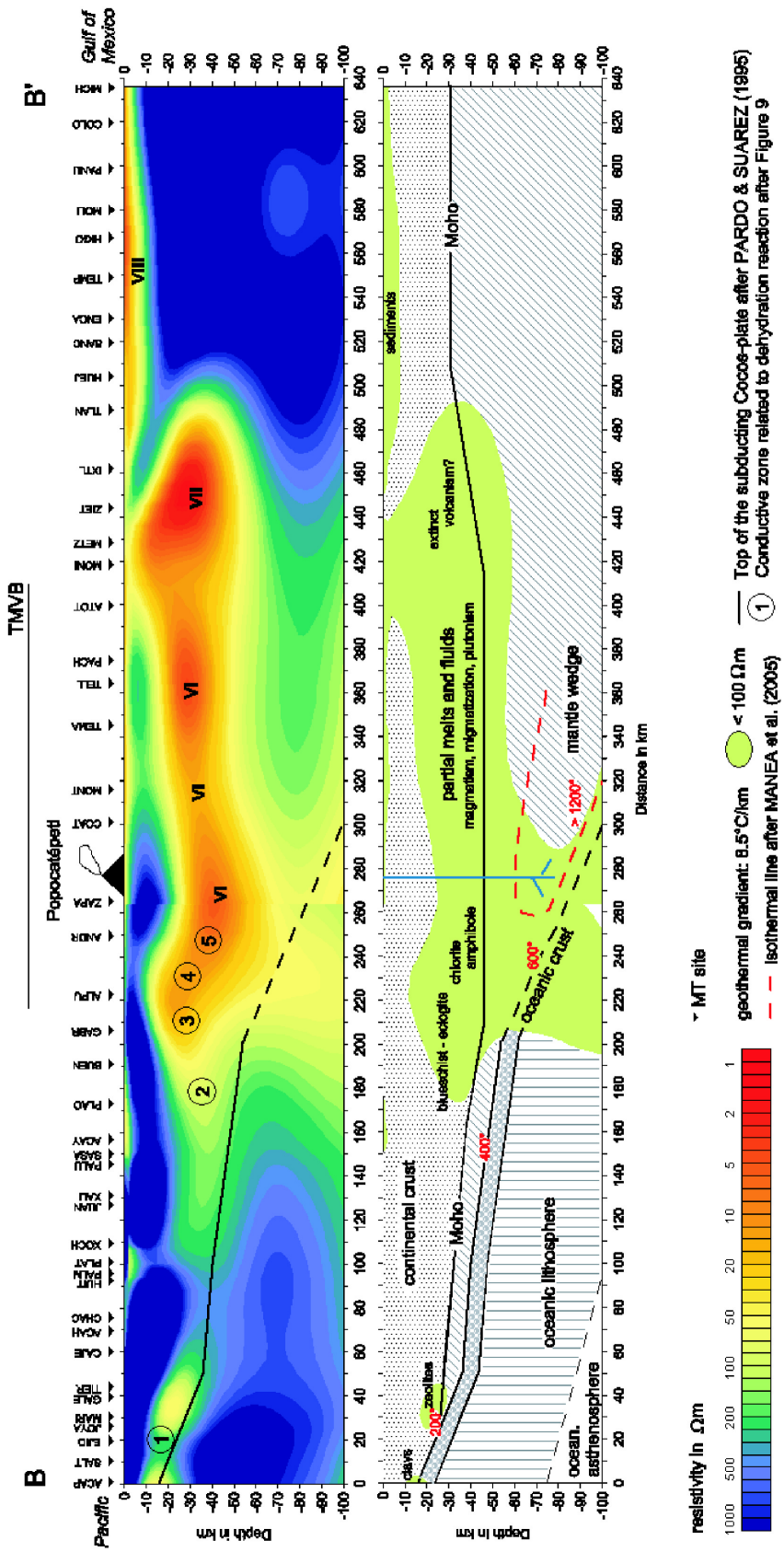


**Figure 12.** Schematic petrological interpretation of conductivity anomalies along MT profile B-B′ (see text); Moho depth after *Ramirez-Ruiz* [1994].

Electronic conductors like black shales would be much more effective in this respect, but deep oil wells in the basin only detected Paleozoic metamorphic or granitic basement at that depth. The downgoing slab has reached the depth of 80 to 90 km at the profile distance around 400 km with temperatures exceeding 1200°C in the intervening mantle wedge (Figure 9). The presence of the nearby late Miocene Anegada High submarine volcanic complex and the active Los Tuxtlas volcanic field, both possibly marking the easternmost extension of the TMVB (Figure 3), may indicate that temperature and hydration conditions are met here to generate mantle melting. The deep crustal high conductance at the northern end of profile A-A′ may thus be related to features that dominate the conductivity structure of profile B-B′ to a great extent.

### 3.5. Conductivity Structure and Dehydration Reactions Along Profile B-B′

[30] If the same geotherm of 8.5°C/km is applicable for an analogous interpretation of the conductivity distribution along profile B-B′ as well, then the same relationships between zones of enhanced conductivity and dehydration reactions should be recognized along this northern profile after adjustments are made for the depth of the subducting slab, using the values from the seismological model of *Pardo and Suarez* [1995]. Thus the small fields of enhanced conductivity near the coast (conductive zone 1, km 0 to 10 and km 25 to 45; Figure 12) may again be attributed either to free water released from open pore space or to crystal or interlayer water released during decomposition of clays and zeolites (dehydration reaction 1, Figure 9). The next dehydration reactions are shifted more inland because of the flatter subduction angle of 10° in the fore-arc region of profile B-B′. The conductivity anomalies produced by the lawsonite blueschist → epidote and epidote blueschist → eclogite transitions (dehydration reactions 2 and 3 in Figure 9) would start at about profile km 175 and km 215, where the conductivity is increased in steps (conductive zones 2 and 3). Because of the inferred down bending of the subducting slab, the breakdown of chlorite (reaction 4) and the decomposition of amphibole (reaction 5) follow at a reduced distance (km 235, zones 4and 5). Therefore reactions 3 to 5 seem to be responsible for one single maximum conductive zone at relatively shallow depths (15 to 30 km). The conductive zones 4 and 5 appear beneath the southwestern part of the TMVB, in the range of the active monogenetic volcanism of Sierra Chichinautzin, which marks the active volcanic front [*Marquez et al.*, 1999; *Wallace and Carmichael*, 1999] (Figure 2). The Popocatépetl active stratovolcano is also located just to the north of the conductive zone 5. However, the lateral extent of the melt region that feeds a stratovolcano can exceed 10 km [*Cañon-Tapia and Walker*, 2004]. Therefore at least part of the conductive zone 5 may be related to melts feeding Popocatépetl. These conductive zones merge into the long significant conductivity anomaly underneath the TMVB (conductive zones VI, VII) that can be attributed to melts, at least in part.

[31] Conductive zone VIII, situated at the northeastern end of profile B-B′, is clearly unrelated to the subduction process. This zone represents the near-surface sedimentary filling of the northern part of the Veracruz basin and may be regarded as an equivalent structure as the conductive zone VIa on profile A-A′.

### 3.6. Origin of Conductivity Anomalies and Water Budget

[32] This overall congruence between the zones of increased conductivity in the continental crust and the positions of important dehydration reactions in the underlying oceanic crust along both MT profiles A-A′ and B-B′ encourages further considerations concerning the origin of conductivity anomalies and the water budget in the fore-arc region of the subduction system. In the near-trench section of the subducting oceanic crust, released water will in part migrate along the interface between slab and overlying continental crust and mantle [*Hensen et al.*, 2004; *Gerya et al.*, 2004]. At greater depths, however, water will ascend into the crust above the slab. The necessary pore space is thought to have opened initially by hydraulic fracturing associated with the dehydration reactions and then held open by the high pressure of the supercritical aqueous metamorphic fluids. The high conductance values of the conductivity anomalies along profile A-A′ suggest that the rising fluids may be stored below an impermeable layer and thus trapped within the middle crust, as proposed by *Hyndman* [1988] for the landward dipping zone of enhanced conductivity on the Lithoprobe profile [*Kurtz et al.*, 1986]. However, in contrast to the Lithoprobe profile, the conductivity structures on profile A-A′ are shallower and thus colder. In particular, the upper boundaries of the conductivity anomalies do not follow any geotherm (Figure 10). Thus the concept of one specific mineral reaction acting as a sealing mechanism may not be applicable here. Instead, the upper and middle crust may possess a low permeability as a whole. The relatively low conductance values near the coast on profile B-B′ might indicate somewhat higher permeability of the overlying crust in this area, possibly allowing part of the water to escape to the surface or else, a larger amount of scraped off sediments might have reduced the available free pore water to be released.

[33] The uptake of water by the deep continental crust may be complicated by multiple hydration-dehydration reactions which may trigger partial melting. In particular, hot dry granulitic rocks at the base of the crust will be readily hydrated or migmatized if free water is available. Thus the mere existence of water-related conductivity anomalies as assumed in our model clearly indicates a surplus of free water implying that the process of hydration of the deep continental crust is fully completed.

[34] For a rough estimate of the pore space needed to explain the zones of enhanced conductivity by free water in interconnected pores, we applied *Archie*'s [1942] power law in its simplest form as commonly used for crystalline rocks [e.g., *Brace*, 1971]

$$\rho_o = \rho_w\left(1/\Phi^2\right)$$

with $\rho_o$ bulk rock resistivity, $\rho_w$ pore water resistivity, and $\Phi$ (open) porosity. In our case, both porosity and pore water resistivity are poorly constrained and this law can only be viewed as simplified description of the bulk rock resistivity. Fluid inclusions in crystalline rocks show a wide range of salinities from less or equivalent to seawater (~35 g/L) up

to oversaturation [*Roedder*, 1984], giving some clue that salinities might rather be high than low. The corresponding resistivities may be extrapolated from experiments on low-salinity fluids [cf. *Quist et al.*, 1970] that show a decrease of resistivity by a factor of ~5 compared to surface values for a fluid at deep crustal temperature and quasi-lithostatic pressure conditions. The latter is needed to keep the pore space open. Taking zones 2 + 3 on profile A-A′ as an example (conductance 2000 S, mean thickness 20 km, i.e., $\rho_o$ = 10 Ω m), an average porosity of $\Phi \approx 8\%$ is estimated for a given pore fluid salinity equivalent to seawater ($\rho_w$ = 0.06 Ω m, extrapolated from seawater resistivity 0.3 Ω m at 25°C). An increase of fluid salinity up to 60 g/l (equivalent to $\rho_w$ = 0.01 Ω m, extrapolated from 0.05 Ω m at 25°C) would result in a porosity of $\Phi \approx 3\%$ which seems to be more realistic. Such salinities have been reported from crystalline rocks at 4000 m depth of the German superdeep borehole (KTB), possibly still increasing by a factor of 1.5 toward the bottom at 9101 m [*Huenges et al.*, 1997] which would further lower the needed porosity to 2.5%. For comparison, quite similar values of 1 to 2% up to 10% porosity were deduced from MT models for the crust above the subducting Juan de Fuca plate in the Lithoprobe and EMSLAB studies [*Hyndman*, 1988; *Kurtz et al.*, 1986; *Wannamaker et al.*, 1989].

[35] The calculated porosities allow estimating the total pore water content of the anomaly, which adds up to $1.6 \times 10^9$ g $H_2O$ $m^{-2}$ for $\Phi \approx 8\%$ or to $0.6 \times 10^9$ g $H_2O$ $m^{-2}$ for $\Phi \approx 3\%$. The latter amount just balances the content of 0.5–$0.6 \times 10^9$ g $H_2O$ $m^{-2}$ of water bound in the basaltic part of the oceanic crust according to *Schmidt and Poli's* [1998] data, which are released at the blueschist (LB + EB) → eclogite transition. Taking the dewatering rate of $0.8 \times 10^7$ g $H_2O$ $m^{-2}$ $km^{-1}$ [*Schmidt and Poli*, 1998] and the convergence rate of 5 cm $yr^{-1}$, the time to generate ("fill") the pore space of the conductivity anomaly would be of the order of 1 Myr if multiple hydration-dehydration reactions or loss of water to the surface are disregarded. Such long residence times would support the above model of an impermeable middle crust at least for the range of the high conducting zones 1–4 on profile A-A′.

### 3.7. Conductivity Structure and Melts Along Profile B-B′

[36] The most significant feature on profile B-B′ is the elongated zone of enhanced conductivity, starting at about 40 km south of the Quaternary TVMB and extending about 40 km to the north of it (Figure 12). As shown in Figure 2, the TMVB consists of andesitic to dacitic stratovolcanoes, fields of monogenetic cones and small lava cones as well as silicic dome complexes and ignimbrites along the profile. The volcanic front is defined by the active stratovolcanoes Popocatépetl and Nevado de Toluca [*García-Palomo et al.*, 2002a] and the Holocene Sierra de Chichinautzin monogenetic volcanic field between them (Figure 2). The Pleistocene Apan volcanic field [*García-Palomo et al.*, 2002b] and the Acoculco caldera [*López-Hernandez and Castillo-Hernandez*, 1997] are situated in the rear part of the arc. Mafic lavas from the Apan field yielded ages as young as 0.47 Ma [*Carrasco Nuñez et al.*, 1997] and 0.24 Ma [*López-Hernandez and Castillo-Hernandez*, 1997]. Furthermore, *Caballero-Miranda et al.* [1999] reported ~50 ka old pyroclastic fall and surge deposits about 20 km south of Pachuca (Figure 2). These ages demonstrate that late Pleistocene to Holocene volcanism occurred throughout the 180 km wide zone crossed by profile B-B′, matching well with the zone of enhanced conductivity centered at ~30 km in the lower continental crust. Laboratory experiments and numerical models indicate that less than 5% interconnected partial melt may induce a drastic increase in conductivity [*Partzsch et al.*, 2000]. Hence, in general agreement with the interpretations of high-conductivity zones in the southern central Andes underneath the volcanic arc [*Schwarz and Krüger*, 1997] and the Altiplano [*Brasse et al.*, 2002], we conclude that the high conductivity observed in the lower crust beneath the TMVB represents a partially molten zone. This interpretation is supported by a low seismic S wave velocity zone (3.3 km/s) found beneath the TMVB [*Gomberg and Masters*, 1988] and a negative Bouguer anomaly (<200 mGal) which was encountered beneath the central part of the TMVB [*Campos-Enriquez and Sanchez-Zamora*, 2000, and references therein].

[37] The conductivity anomaly, as imaged by the 2-D MT model for profile B-B′, shows some internal structures, for example, a local maximum at km 240–280, which is observed well below the presently active volcanoes. However, little insight is provided into the complex processes of melt generation as indicated by the coexistence of various melt types. Given the geometry of the subducting slab including, in particular, its down bending at km 200, temperatures of 1000°C and more must be reached in the continental mantle wedge just underneath the active volcanic belt assuming strong temperature-dependent viscosity of the mantle (Figure 12), with maximum temperatures of more than 1200°C beneath the Popocatépetl volcano [*Manea et al.*, 2005]. Here, basaltic magmas are generated by melting of the peridotite. Sufficient water to lower the melting temperature is available from the amphibole-out reaction (dehydration reaction/conductive zone 5) and the decomposition of the hydrous phases lawsonite, zoisite, chloritoid, and talc, which in part are still contained in the oceanic crust beyond the blueschist → eclogite transformation [*Schmidt and Poli*, 1998]. During ascent, the primary basalt is modified to andesitic-dacitic compositions as found in recent volcanoes signifying temporary storage and fractional differentiation in magma chambers. Another portion of the ascending basalt may intrude into the lower continental crust or is added to the crust by underplating. There it can cause partial melting of metabasites and metapelites due to its high heat capacity and water content that lowers the melting point of the deep crustal rocks to temperatures as low as 600–650°C [e.g., *Sparks*, 1992]. This can lead to migmatization and rise of granitic melts into midcrustal positions, forming large plutons. Some of the silicic magmas migrate to the surface, where they are found in the TMVB. It should be noted that, due to low resolution, small vertical conductivity structures like dykes or ascending fluid pathways cannot be seen in the MT models. Also, the detection of small-scale magma chambers (~5 km) is impeded because of too large average MT site distances of 10–15 km (Figure 3).

[38] In summary, the high conductance underneath the central part of the TMVB, in particular, the area of recent volcanism (zone VI), is interpreted to be cause by the

presence of partial melts and fluids of various origins, including brines, ongoing migmatization, growing plutons as well as residual metamorphic fluids.

### 3.8. Fossil Melts?

[39] It is not possible to define sharp boundaries for the elongated zone of melt production. To the southwest, the zone obviously merges into an area of enhanced conductivity that has been explained by fluids deriving from near-trench dehydration processes where active volcanism is lacking (zones 2–3). To the northeast of the TMVB, a conductive zone is imaged at km 400–480 (zone VII) showing the absolute conductance maximum on profile B-B′ (>10,000 S) which is more difficult to understand. Uprising fluids from the deeply subducted oceanic crust can be excluded, because there is no recent volcanic activity observable in this area. Three, nonexclusive, possibilities may be considered: (1) "fossil" partial melts and associate metamorphic fluids, (2) fluids in a major shear zone and, (3) graphitic shear zones in the middle and lower crust.

[40] 1. At the surface the region is characterized by alternating mafic-silicic pulses of volcanism (Figure 2). Alkaline basalts were emplaced between 7.5 and 6.5 Ma and were followed at ~5 Ma by silicic ignimbrites and domes [*Cantagrel and Robin*, 1979; *Robin*, 1982; *Ferrari et al.*, 2005]. The latter, in turn, were covered by basaltic andesites about 2.5 Myr ago [*Cantagrel and Robin*, 1979; *Ferrari et al.*, 2005] (Figure 2). Recently, the 7.5–6.5 Ma basaltic volcanism has been considered as the surface expression of a thermal event induced by the detachment of the lower part of the slab in this region [*Ferrari*, 2004]. Therefore repeated magmatic events may have produced partial melts within the crust, which together with relics of metamorphic fluids are still observable in our MT model. Long lasting conductivity anomalies beneath an extinct volcanic field have also been observed in the Canadian Cordillera [*Wennberg et al.*, 2002].

[41] 2. This anomaly also corresponds to a large crustal fault zone bounding the Mexican Altiplano. To the southwest of this zone, Precambrian gneisses are exposed ~500 m above sea level (Huiznopala gneisses [*Lowlor et al.*, 1999]) (Figure 2), whereas correlative rocks were cored at a depth of >2600 m toward the north in the coastal plain of the Gulf of Mexico [*Suter*, 1990]. The fault zone in between (northwest of MT site IXTL) is part of structures that accommodated the opening of the Gulf of Mexico in Jurassic times. Thus the high conductive zone could be due to fluids (brines) migrating upward along this major crustal structure.

[42] 3. The high conductivity in this area may reflect the presence of graphite in the underlying Precambrian crust. Indeed the Grenvillian granulite facies Huiznopala gneisses are discontinuously exposed just to the west of the B-B′ profile between km 450 and 490. According to *Lowlor et al.* [1999] the largest outcrop consists of paragneisses dominated by graphite-rich calc-silicate gneisses. The role of graphite in enhancing electrical conductivity in deep crustal rocks has been put forward both in laboratory experiments and field case studies [*Haak et al.*, 1997; *Duba et al.*, 2001]. Normally, graphite in the deep crust is expected to exist in the form of isolated grains, which do not contribute much to the bulk conductivity. In shear zones, however, high conductivity may either be produced by graphite precipitation from C-O-H fluids, which may form interconnected films covering the shear planes, or by large amounts of synsedimentary graphite grains, that are sheared/smeared together by the shear process forming an interconnected network as well [*Jödicke et al.*, 2004; *Nover et al.*, 2005].

[43] Regarding the regional extent and the unusually high conductance of that anomaly, we may favor the explanation of residual fossil melts/fluids beneath the extinct volcanic field, possibly in association with the effects of large shear zones. If this interpretation is correct, it remains unclear which processes associated with extinct volcanism could cause the particularly high conductance values compared to active volcanic processes. Interestingly, the similarly large anomaly observed at the northeastern end of profile A-A′ (conductive zones VIa + VIb, total conductance >8000 S, Figures 6 and 11) was interpreted to be related to the late Miocene Anegada High submarine volcanic complex and to the Los Tuxtlas volcanic field (Figure 3). The Anegada High consists of basaltic flows and breccias, detected in exploratory wells and seismic lines, and is situated between the easternmost end of the TMVB and the late Miocene to Quaternary Los Tuxtlas volcanic field [*Jennette et al.*, 2003; *Ferrari et al.*, 2005]. Volcanism in the Los Tuxtlas field started at ~7 Ma and is still active, as witnessed by the historic eruptions of the San Martín volcano in 1664 and 1793 [*Nelson and Gonzalez-Craver*, 1992]. On the basis of detailed petrologic studies *Nelson et al.* [1995] concluded that the Los Tuxtlas volcanism is subduction-related. Furthermore, the Anegada High and the Los Tuxtlas volcanic field are located along the prominent, NW trending transcurrent fault system of the Anton Lizardo lineaments, which were active in the Neogene [*Jennette et al.*, 2003]. Thus, beside recent volcanic activity, the deep crustal high conductance on profile A-A′ detected in this area may be due to fossil volcanic activity and the presence of a major crustal shear zone as well, resembling herein the conductive zone VII on profile B-B′.

## 4. Conclusions

[44] The main result of this MT study in southern Mexico is the detection of distinct patterns of high-conductivity zones in the deep continental crust along the two coast to coast profiles A-A′ and B-B′. For the fore-arc region of the Cocos plate subduction system, this pattern is basically assumed to originate from ascending fluids released by major dehydration reactions at specific p-T conditions of the underlying oceanic crust, whereas the downgoing plate itself is not detectable electrically. This situation differs, for example, from the setting along the west coast of North America in Oregon, where a dipping layered conductive structure appears at larger depths and seems to delineate the top of the Juan de Fuca plate [*Wannamaker et al.*, 1989].

[45] The presence of more or less isolated conductivity anomalies particularly on profile A-A′ offers the rare opportunity to recognize the sequence of the main dehydration reactions and, moreover, to estimate the thermal gradient at the top of the subducting oceanic crust by directly correlating the locations of the deep continental high-conductivity zones with these reactions. From this correlation a thermal gradient of about 8.5°C/km results

for the manual best fit. By thermomechanical modeling the thermal structure of the subducted plate for the actual parameters set of profile A-A′ such a moderate gradient can only be achieved if additional heat sources like shear heating are implemented.

[46] The estimated value of a moderate geotherm appears meaningful, because it allows assigning the conductivity anomalies along profile B-B′ basically to the same system of metamorphic reactions that was used to explain profile A-A′. Moreover, together with geometrical factors it gives the clue for the understanding of the fundamental difference observed along the two MT profiles, namely the generation of melts and the formation of the Trans-Mexican Volcanic Belt on profile B-B′; and the lack of those on profile A-A′.

[47] Profile A-A′ shows a situation typical for a young oceanic lithosphere. Given the geometry of a near-trench moderate dip of the subducting plate (13°) and a slight up bending near the center of the profile, dehydration reactions occur relatively close to the coast. Producing remarkable conductivity anomalies, the water is released almost at the contact with the continental crust or with the cold corner of the mantle wedge, the temperatures of which are insufficient to produce any melting.

[48] In comparison, the dip of the Cocos plate along profile B-B′ (10°) is slightly flatter in the fore-arc region. This leads to a shift of the main dehydration reactions to more inland positions. In sharp contrast, the steep down bending of the plate near the volcanic front forces dewatering at a remarkably reduced distance along the profile. The broad conductivity anomaly observed in this section may be interpreted to originate from various successive reactions. Sufficient water potential seems to be kept that allows initiating melting of the hot mantle material after the plate has reached a depth of 80 km at 260 km profile distance. At much larger distance from the trench, this crucial range is reached on profile A-A′ at the profile distance of about 400 km. Approaching the easternmost end of the TMVB, the sparse historical volcanism of the nearby Los Tuxtlas volcanic field indicates that appropriate conditions for the generation of mantle melting are met here as well. Thus, by the formation of a well-defined volcanic belt the subduction of the Cocos plate along profile B-B′ resembles more a cold subduction, in contrast to the warm subduction of the Cocos plate along profile A-A′. We may conclude that this difference is mainly due to the different geometrical settings, in particular, to the down and up bending of the plate in the fore-arc region, which seem to affect the dehydration kinetics. Other parameters like distance from the coast, temperature and depth are almost identical for the respective regions, where volcanism is generated on profile B-B′ but lacking on profile A-A′.

[49] In the MT model of profile B-B′, the conductivity anomalies which appear to be directly associated with the TMVB are concentrated in the middle and deep continental crust. The recently active volcanic front correlates with a maximum of regional conductance, but little is known about the structure of ongoing magmatism and plutonism. We may assume that this is due to the fact that partial melts and fluids of various origins cover a similar parameter range of electrical conductivity, which does not support any detailed recognition of the assumed complex system of superimposed internal processes. Moreover, any clear distinction between active and extinct volcanic activity may be obscured by fossil melts and metamorphic fluids that seem to keep or even to reinforce their electrical properties during long time residence in the deep crust. At larger depths, neither the region of basaltic melt generation nor the paths of uprising magma in the intervening continental mantle wedge are clearly imaged. This may be due to the shielding effect of the overlying high-conductivity zone and by general limitations of the MT method with regard to the resolution of vertical structures.

[50] Beyond such limitations, the application of the magnetotelluric method to an active subduction zone may have demonstrated again that it is extremely promising to utilize the variety of electrical conductivity signatures observable in such an environment, the analysis of which may contribute in a very specific way to a better understanding of the relationships between tectonics, material transport and metamorphic processes.

[51] **Acknowledgments.** This work was initiated by R. Meißner and H. Böhnel (GEOLIMEX Group) and supported by the Deutsche Forschungsgemeinschaft (DFG) and the Universidád Autónoma de México (UNAM) under grants Jo 188/1–1-5, PAPIIT-IN119197, and ES102801, which is gratefully acknowledged. We are greatly indebted to T. Allgeier, B. Bartling, J. Mührs, M. Pareja Lopez, E. Rionda Morfin, V. Schäpe, F. Schmieder, and K. Strobeck, who took part in the fieldwork. K. Bahr gave us valuable advice how to decompose our data. Our work benefited from fruitful discussions with H. Böhnel, V. Kostoglodov, P. Schaaf, S. K. Singh, J. Urrutia-Fucugauchi, R. Zuniga, and M. Guzman, who also provided the earthquake data along the two MT profiles. J. Untiedt is thanked for careful reading of the manuscript and his steady support of the project. The constructive comments of two reviewers helped to improve the manuscript.

## References

Archie, G. E. (1942), The electrical resistivity log as an aid in determining some reservoir characteristics, *Trans. Am. Inst. Min. Metall. Pet. Eng.*, *146*, 54–62.

Arzate, J. A., M. Mareschal, and D. Livelybrooks (1995), Electrical image of the subducting Cocos plate from magnetotelluric observations, *Geology*, *23*, 703–706.

Austrheim, H., and T. M. Boundy (1994), Pseudotachylites generated during seismic faulting and eclogitization of the deep crust, *Science*, *265*, 82–83.

Bahr, K. (1988), Interpretation of the magnetotelluric impedance tensor: Regional induction and local telluric distortion, *J. Geophys.*, *62*, 119–127.

Bahr, K. (1991), Geological noise in magnetotelluric data: A classification of distortion types, *Phys. Earth Planet. Inter.*, *66*, 24–38.

Böhnel, H. (1985), Palaomagnetische Untersuchungen and jurassischen bis quartaren Gesteinen aus Zentral- und Sudmexico, dissertation, Inst. for Geophys., Univ. Muenster, Muenster, Germany.

Boundy, T. M., D. M. Fountain, and H. Austrheim (1992), Structural development and petrofabrics of eclogite facies shear zones, Bergen arcs, western Norway: Implications for deep crustal deformational processes, *J. Metamorph. Geol.*, *10*, 127–146.

Brace, W. F. (1971), Resistivity of saturated crustal rocks to 40 km based on laboratory measurements, in *The Structure and Physical Properties of theEarth's Crust*, *Geophys. Monogr. Ser.*, vol. 14, edited by J. G. Heacock pp. 243–255, AGU, Washington, D. C.

Brasse, H., P. Lezaeta, V. Rath, K. Schwalenberg, W. Soyer, and V. Haak (2002), The Bolivian Altiplano conductivity anomaly, *J. Geophys. Res.*, *107*(B5), 2096, doi:10.1029/2001JB000391.

Caballero-Miranda, M., S. Lozano, B. Ortega, J. Urrutia-Fucugauchi, and J. L. Macias (1999), Environmental characteristics of Lake Tecocomulco, northern basin of Mexico, for the last 50,000 years, *J. Paleolimnol.*, *22*, 399–411.

Campa, M. F., and P. J. Coney (1983), Tectono-stratigraphic terranes and mineral resource distributions in Mexico, *Can. J. Earth Sci.*, *20*, 1040–1051.

Campos-Enríquez, J. O., and O. Sanchez-Zamora (2000), Crustal structure across southern Mexico inferred from gravity data, *J. S. Am. Earth Sci.*, *13*, 479–489.

Cañón-Tapia, E., and G. P. L. Walker (2004), Global aspects of volcanism: The perspectives of ''plate tectonics'' and ''volcanic systems'', *Earth Sci. Rev.*, *66*, 163–182.

Cantagrel, J. M., and C. Robin (1979), K-Ar dating on eastern Mexican volcanic rocks—Relations between the andesitic and alkaline provinces, *J. Volcanol. Geotherm. Res.*, *5*, 99–114.

Carrasco Nuñez, G., A. Gómez Tuena, and L. Lozano Vasquez (1997), Geological map of the Cerro Grande volcano and surrounding area, central Mexico, *Geol. Soc. Am. Map Chart Ser., MCH 083*, 16 pp.

de Graciansky, P. C., G. Deroo, J. P. Herbin, L. Montadert, C. Müller, A. Schaaf, and J. Sigal (1984), Ocean-wide stagnation episode in the late Cretaceous, *Nature*, *308*, 346–349.

Duba, A. G., E. A. Mathez, and T. J. Shankland (2001), Workshop addresses crustal carbon and its effect on electrical conductivity, *Eos Trans. AGU*, *82*, 456.

Evans, B. W. (1990), Phase relations of epidote blueschists, *Lithos*, *25*, 3–23.

Ferrari, L. (2004), Slab detachment control on volcanic pulse and mantle heterogeneity in central Mexico, *Geology*, *32*, 77–80.

Ferrari, L., M. Lopez-Martinez, G. Aguirre-Diaz, and G. Carrasco-Nuñez (1999), Space-time patterns of Cenozoic arc volcanism in central Mexico: From the Sierra Madre Occidental to the Mexican Volcanic Belt, *Geology*, *27*, 303–307.

Ferrari, L., J. Rosas Elguera, G. Carrasco Nuñez, T. Norato Cortez, and N. Gonzalez Cervantes (2002), Digital geologic cartography of the Trans-Mexican Volcanic Belt and adjoining areas: An illustrated summary of the evolution of Neogene volcanism in central Mexico, paper presented at III Reunion Nacional de Ciencias de la Tierra, Union Geofis. Mex., Puerto Vallarta, México.

Ferrari, L., T. Tagami, M. Eguchi, M. T. Orozco-Esquivel, C. M. Petrone, J. Jacobo-Albarrán, and M. López-Martínez (2005), Geology, geochronology and tectonic setting of late Cenozoic volcanism along the southwestern Gulf of Mexico: The eastern alkaline province revised, *J. Volcanol. Geotherm. Res.*, *146*, 284–306.

García-Palomo, A., J. L. Macías, J. L. Arce, L. Capra, V. H. Garduño, and J. M. Espíndola (2002a), Geology of Nevado de Toluca volcano and surrounding areas, central Mexico, *Geol. Soc. Am. Map Chart Ser.*, *MCH 089*, 26 pp.

García-Palomo, A., J. L. Macías, G. Tolson, G. Valdez, and J. C. Mora (2002b), Volcanic stratigraphy and geological evolution of the Apan region, east-central sector of the Trans-Mexican Volcanic Belt, *Geofis. Int.*, *41*, 1–18.

GEOLIMEX Working Group (1994), Reflection of the subducting plate? First results of a Mexican geotraverse, *Z. Geol. Paläontol.*, *1*, 541–553.

Gerya, T. V., D. A. Yuen, and E. O. D. Sevre (2004), Dynamical causes for incipient magma chambers above slabs, *Geology*, *32*, 89–92.

Gomberg, J., and T. G. Masters (1988), Waveform modeling using locked-mode synthetic and differential seismograms: Application to determination of the structure of Mexico, *Geophys. J. R. Astron. Soc.*, *94*, 1–20.

Groom, R. W., and R. C. Bailey (1989), Decomposition of the magnetotelluric impedance tensor in the presence of local three dimensional galvanic distortion, *J. Geophys. Res.*, *94*, 1913–1925.

Haak, V., et al. (1997), KTB and the electrical conductivity of the crust, *J. Geophys. Res.*, *102*, 18,289–18,305.

Hensen, C., K. Wallmann, M. Schmidt, C. R. Ranero, and E. Suess (2004), Fluid expulsion related to mud extrusion off Costa Rica—A window to the subducting slab, *Geology*, *32*, 201–204.

Huenges, E., J. Erzinger, J. Kück, B. Engeser, and W. Kessels (1997), The permeable crust: Geohydraulic properties down to 9101 m depth, *J. Geophys. Res.*, *102*, 18,255–18,265.

Hyndman, R. D. (1988), Dipping seismic reflectors, electrically conductive zones, and trapped water in the crust over a subducting plate, *J. Geophys. Res.*, *93*, 13,391–13,405.

Ingham, M. R. (1988), A magnetotelluric and magnetovariational traverse across the New Zealand subduction zone, *Geophys. J.*, *92*, 495–504.

Iwamori, H. (1998), Transportation of $H_2O$ and melting in subduction zones, *Earth Planet. Sci. Lett.*, *160*, 65–80.

Jennette, D., T. Wawrzyniec, K. Fouad, D. Dunlap, J. Meneses-Rocha, F. Grimaldo, R. Muñoz, D. Barrera, C. Williams-Rojas, and A. Escamilla-Herrera (2003), Traps and turbidite reservoir characteristics from a complex and evolving tectonic setting, Veracruz Basin, southeastern Mexico, *AAPG Bull.*, *87*, 1599–1622.

Jödicke, H., J. H. Kruhl, C. Ballhaus, P. Giese, and J. Untiedt (2004), Syngenetic, thin graphite-rich horizons in lower crustal rocks from the Serre San Bruno, Calabria (Italy), and implications for the nature of high-conducting deep crustal layers, *Planet. Earth Phys. Inter.*, *141*, 32–58.

Jones, A. G. (1993), Electromagnetic images of modern and ancient subduction zones, *Tectonophysics*, *219*, 29–45.

Jording, A. (2000), Die Verteilung der elektrischen Leitfahigkeit in der Kruste und im oberen Mantel under Sudmexiko im Krustenbereich der subduzierten Cocos Platte, dissertation, Inst. for Geophys., Univ. Muenster, Muenster, Germany.

Jording, A., L. Ferrari, J. Arzate, and H. Jödicke (2000), Crustal variations and terrane boundaries in southern Mexico as imaged by magnetotelluric transfer functions, *Tectonophysics*, *327*, 1–13.

Kerrick, D. M., and J. A. Connolly (2001), Metamorphic devolatilization of subducted oceanic metabasalts: Implications for seismicity, arc magmatism and volatile recycling, *Earth Planet. Sci. Lett.*, *189*, 19–29.

Kirby, S., E. R. Engdahl, and R. Denlinger (1996), Intermediate-depth intraslab earthquakes and arc volcanism as physical expressions of crustal and uppermost mantle metamorphism in subducting slabs, in *Subduction: Top to Bottom*, *Geophys. Monogr. Ser.*, vol. 96, edited by G. E. Bebout et al., pp. 195–214, AGU, Washington, D. C.

Kurtz, R. D., J. M. DeLaurier, and J. C. Gupta (1986), A magnetotelluric sounding across Vancouver Island detects the subducting Juan de Fuca plate, *Nature*, *321*, 596–599.

Kurtz, R. D., J. M. DeLaurier, and J. C. Gupta (1990), The electrical conductivity distribution beneath Vancouver Island: A region of active plate subduction, *J. Geophys. Res.*., *95*, 10,929–10,949.

López-Hernandez, A., and D. Castillo-Hernandez (1997), Exploratory drilling at Acoculco, Puebla, México: A hydrothermal system with only nonthermal manifestation, *Geotherm. Res. Counc. Trans.*, *21*, 429–433.

Lowlor, P. J., F. Ortega-Gutierrez, K. L. Cameron, H. Ochoa-Camarillo, R. Lopez, and D. E. Sampson (1999), U-Pb geochronology, geochemistry and provenance of the Grenvillian Huiznopala Gneiss of eastern Mexico, *Precambrian Res.*, *94*, 73–99.

Mackie, R., S. Rieven, and W. Rodi (1997), Users manual and software documentation for two-dimensional inversion of magnetotelluric data, 14 pp., Mass. Inst. of Technol., Earth Resour. Lab., Cambridge.

Manea, V. C., M. Manea, V. Kostoglodov, and G. Sewell (2005), Thermomechanical model of the mantle wedge in central Mexican subduction zone and a blob tracing approach for the magma transport, *Phys. Earth Planet. Inter.*, *149*, 165–186.

Marquez, A., S. P. Verma, F. Anguita, R. Oyarzun, and J. L. Brandle (1999), Tectonics and volcanism of Sierra Chichinautzin: Extension at the front of the Central Trans-Mexican Volcanic belt, *J. Volcanol. Geotherm. Res.*, *93*, 125–150.

Nelson, S. A., and E. Gonzalez-Caver (1992), Geology and K-Ar dating of the Tuxtla Volcanic Field, Veracruz, Mexico, *Bull. Volcanol.*, *55*, 85–96.

Nelson, S. A., E. Gonzalez-Caver, and K. Kyser (1995), Constraints on the origin of alkaline and calc-alkaline magmas from Los Tuxtlas volcanic field, Veracruz Mexico, *Bull. Volcanol.*, *122*, 191–211.

Nixon, G. T. (1988), Petrology of the younger andesites and dacites of Iztaccihuatl volcano, Mexico: II. Chemical stratigraphy, magma mixing, and the composition of basaltic magma influx, *J. Petrol.*, *29*, 265–303.

Nover, G., J. Stoll, and J. von der Gönna (2005), Promotion of graphite formation by tectonic stress–a laboratory experiment, *Geophys. J. Int.*, *160*(3), 1059–1067, doi:10.1111/j.1365-246X.2005.02395.x.

Ortega-Guiterres, F., R. L. Sewdlock, and R. C. Speed (1994), Phanerozoic tectonic evolution of Mexiko, in *Phanerozoic Evolution of North American Continent-Ocean Transitions*, edited by R. C. Speed, pp. 265–306, Geol. Soc. of Am., Boulder, Colo.

Pardo, M., and G. Suarez (1995), Shape of the subducted Rivera and Cocos plates in southern Mexico: Seismic and tectonic implications, *J. Geophys. Res.*., *100*, 12,357–12,373.

Partzsch, G. M., F. R. Schilling, and J. Arndt (2000), The influence of partial melting on the electrical behavior of crustal rocks: Laboratory examinations, model calculations and geological interpretations, *Tectonophysics*, *317*, 189–203.

Peacock, S. M. (1990), Fluid processes in subduction zones, *Science*, *248*, 329–337.

Peacock, S. M. (1991), Numerical simulation of subduction zone pressure-temperature-time paths: Constraints on fluid production and arc magmatism, *Philos. Trans. R. Soc. London, Ser. A*, *335*, 341–353.

Peacock, S. M. (1992), Blueschist-facies metamorphism, shear heating, and p-T-t paths in subduction shear zones, *J. Geophys. Res.*, *97*, 17,693–17,707.

Peacock, S. M. (1993), The importance of blueschist-eclogite dehydration reactions in subducting oceanic crust, *Geol. Soc. Am. Bull.*, *105*, 684–694.

Peacock, S. M. (1996), Thermal and petrological structure of subduction zones, in *Subduction Top to Bottom*, *Geophys. Monogr. Ser.*, vol. 96, edited by G. E. Bebout et al., pp. 119–134, AGU, Washington, D. C.

Peacock, S. M., and K. Wang (1999), Seismic consequences of warm versus cool subduction metamorphism: Examples from southwest and northeast Japan, *Science*, *286*, 937–939.

Peacock, S. M., T. Rushmer, and A. B. Thompson (1994), Partial melting of subducting oceanic crust, *Earth Planet. Sci. Lett.*, *121*, 227–244.

Poli, S., and M. W. Schmidt (1995), $H_2O$ transport and release in subduction zones: Experimental constraints on basaltic and andesitic systems, *J. Geophys. Res.*, *100*, 22,299–22,314.

Poli, S., and M. W. Schmidt (2002), Petrology of subducted slabs, *Annu. Rev. Earth Planet. Sci.*, *30*, 207–235.

Quist, A. S., W. L. Marshall, E. U. Franck, and W. von Osten (1970), Reference solution for electrical measurements to 800° and 12000 bars: Aqueous 0.01 Demal potassium chloride, *J. Phys. Chem.*, *74*, 2241–2243.

Ramirez-Ruiz, J. J. (1994), Gravity and seismic interpretation of crustal structures at the pacific continental margin and along the GEOLIMEX transect in southern Mexico, disertation, 144 pp., Christian Albrechts Univ., Kiel, Germany.

Ranero, C. R., J. Phipps Morgan, K. D. McIntosh, and C. Reichert (2003), Bending, faulting, and mantle serpentinization at the Middle America trench, *Nature*, *425*, 367–373.

Robin, C. (1982), Mexico, in *Andesites, Orogenic Andesites and Related Rocks*, edited by R. S. Thorpe, pp. 137–147, John Wiley, Hoboken, N. J.

Rodi, W., and R. L. Mackie (2001), Nonlinear conjugate gradients algorithm for 2-D magnetotelluric inversion, *Geophysics*, *66*, 174–187.

Roedder, E., (Ed.) (1984), *Fluid Inclusions*, *Rev. Mineral.*, vol. 12, Mineral. Soc. of Am., Washington, D. C.

Rüpke, L. H., J. P. Morgan, M. Hort, and J. Connolly (2002), Are the regional variations in Central American arc lavas due to differing basaltic versus peridotitic slab sources of fluids?, *Geology*, *30*, 11,035–11,038.

Rüpke, L. H., J. P. Morgan, M. Hort, and J. Connolly (2004), Serpentine and the subduction zone water cycle, *Earth Planet. Sci. Lett.*, *223*, 17–34.

Russell, M. J. (1992), Plate tectonics and hydrothermal ore deposits, in *Understanding the Earth. A New Synthesis*, edited by G. C. Brown, C. J. Hawkesworth, and R. C. L. Wilson, Cambridge Univ. Press, New York.

Schmidt, M. W., and S. Poli (1998), Experimentally based water budgets for dehydrating slabs and consequences for arc magma generation, *Earth Planet. Sci. Lett.*, *163*, 361–379.

Schwarz, G., and D. Krüger (1997), Resistivity cross section through the southern central Andes as inferred from magnetotelluric and geomagnetic deep sounding, *J. Geophys. Res..*, *102*, 11,957–11,978.

Sheth, H. C., I. S. Torres-Alvarado, and S. P. Verma (2000), Beyond subduction and plumes; a unified tectonic-petrogenetic model for the Mexican volcanic belt, *Int. Geol. Rev.*, *42*, 1116–1132.

Singh, S. K., G. Suarez, and T. Dominguez (1985), The Oaxaca, Mexico, earthquake of 1931: Lithospheric normal faulting in the subducted Cocos plate, *Nature*, *317*, 56–58.

Smith, T., and J. Booker (1991), Rapid inversion of two- and three-dimensional magnetotelluric data, *J. Geophys. Res.*, *96*, 3905–3922.

Sparks, S. J. (1992), Magma generation in the Earth, in *Understanding the Earth: A New Synthesis*, edited by G. C. Brown, C. J. Hawkesworth, and R. C. L. Wilson, pp. 91–114, Cambridge Univ. Press, New York.

Spear, F. S. (1993), *Metamorphic Phase Equilibria and Pressure-Temperature-Time Paths*, 799 pp., Mineral. Soc.of Am., Washington, D. C.

Spranger, M. (1994), GEOLIMEX: Eine erste Geotraverse durch Südmexiko. Auswertung des refraktionsseismischen Profils, dissertation, 150 pp., Christian Albrechts Univ., Kiel, Germany.

Straub, S., and A. L. Martin del Pozzo (2001), The significance of phenocrysts diversity in tephra from recent eruptions at Popocatepetl volcano, central México, *Contrib. Mineral. Petrol.*, *140*, 487–510.

Suarez, G., J. P. Ligorria, and L. Ponce (1992), Preliminary crustal structure of the coast of Guerrero, Mexico, using the minimum apparent velocity of refracted waves, *Geofis. Int.*, *31*, 247–252.

Suter, M. (1990), Geología de la hoja Tamzunchale, estados de Hidalgo, Queretaro y San Luis Potosí, Carta Geologica de México serie de 1:100,000, Univ. Nac. Autón. de Méx., Inst. de Geol., Mexico City.

Swift, C. M. (1967), A magnetotelluric investigation of an electrical conductivity anomaly in the southwestern United States, Ph.D. thesis, Geophys. Lab., Mass. Inst. of Technol., Cambridge.

Tatsumi, Y., and S. Eggins (1995), *Subduction Zone Magmatism*, 211 pp., Blackwell, Malden, Mass.

Valdez-Gonzalez, C., and R. P. Meyer (1996), Seismic structure between the Pacific coast and Mexico City from the Petatlan earthquake (*Ms* = 7.6) aftershocks, *Geofis. Int.*, *35*, 377–401.

van Keken, P. E., B. Kiefer, and S. M. Peacock (2002), High-resolution models of subduction zones: Implications for mineral dehydration reactions and the transport of water into the deep mantle, *Geochem. Geophys. Geosyst.*, *3*(10), 1056, doi:10.1029/2001GC000256.

Wallace, P. J., and I. S. E. Carmichael (1999), Quaternary volcanism near the Valley of Mexico: Implications for subduction zone magmatism and the effects of crustal thickness variations on primitive magma compositions, *Contrib. Mineral. Petrol.*, *135*, 291–314.

Wang, K., R. D. Hyndman, and M. Yamano (1995), Thermal regime of the southwest Japan subduction zone: Effects of age history of the subducting plate, *Tectonophysics*, *248*, 53–69.

Wannamaker, P. E., J. R. Booker, A. G. Jones, A. D. Chave, J. H. Filloux, H. S. Waff, and L. K. Law (1989), Resistivity cross section through the Juan de Fuca subduction system and its tectonic implications, *J. Geophys. Res.*, *94*, 14,127–14,144.

Wennberg, G., I. J. Ferguson, J. Ledo, and A. G. Jones (2002), Northern Cordillera Crustal Structure: SNORCLE. Corridor 2, paper presented at 16th Workshop on Electromagnetic Induction in the Earth, Woods Hole Oceanogr. Inst., Santa Fe, N. M.

J. Arzate and L. Ferrari, Centro de Geociencias, Campo Juriquilla, UNAM, Apdo. Postal 1-742, 76001 Querétaro, México.

A. Jording, Institut für Geophysik der Westfälischen Wilhelms-Universität Münster, Corrensstr. 24, D-48149 Münster, Germany.

K. Mezger, Institut für Mineralogie der Westfälischen Wilhelms-Universität Münster, Corrensstr. 24, D-48149 Münster, Germany. (klaush@nwz.uni-muenster.de)

L. Rüpke, SFB 574 und IFM-GEOMAR, Leibniz-Institut für Meereswissenschaften an der Universität Kiel, Wischhofstraße 1-3, D-24148 Kiel, Germany.